A VIRTUAL PIVOT POINT APPROACH TO THE CONTROL OF QUADRUPEDAL ROBOT RUNNING

by

GilHwan Kim

A thesis submitted to the Faculty of the University of Delaware in partial fulfillment of the requirements for the degree of Master of Science in Mechanical Engineering

Winter 2020

A VIRTUAL PIVOT POINT APPROACH TO THE CONTROL OF QUADRUPEDAL ROBOT RUNNING

by

GilHwan Kim

Approved: _____
Ioannis Poulakakis, Ph.D.
Professor in charge of Advisory Committee

Approved: _____
Ajay Prasad, Ph.D.
Chair of the Department of Mechanical Engineering

Approved: _____
Levi Thompson, Ph.D.
Dean of the College of Engineering

Approved: _____
Douglas J. Doren, Ph.D.
Interim Vice Provost for Graduate and Professional Education and
Dean of the Graduate College

ACKNOWLEDGMENTS

First of all, I would like to appreciate my advisor Dr. Poulakakis for his plenty of guidance toward this research. His exceptional perspective, knowledge, and energy not only encouraged me to challenge the difficult research problem but also provided a valuable model to be a good researcher.

I would also like to thank all my friends in the lab directly or indirectly contributed to my thesis completion. Thanks to Prem for our discussion and my roommate Woosik for taking care of me, despite his tight schedule.

Outside the lab, thanks to the pastor and my friends for their prayer and concern which were a great help in my study abroad life. Without their help, it would be hard to settle down in Newark.

This thesis is dedicated to my family. Thanks to my brother for his encouragement during his hard and busy times. I appreciate my parents more than I can express for their support and great love in my life. Their care and encouragement made me overcome every hard time that I encountered.

TABLE OF CONTENTS

LIST OF TABLES

LIST OF FIGURES

ABSTRACT

Despite significant progress on wheeled vehicles, a large portion of earth landmass is limited to the wheeled robots. Legged robots provide an attractive alternative to address mobility limitations in extreme terrain environments. Much of the effort on legged robots has been concentrated on quadrupeds due to their inherent stability characteristics.

In this thesis, we focus on running quadrupeds with a bounding gait. We propose a discrete-time control approach that stabilizes periodic bounding gaits that take advantage of the passive dynamics of the system. The proposed controller uses the concept of a Virtual Pivot Point (VPP) within a discrete Linear Quadratic Regulator (LQR) to enhance bounding stability. In our approach, stability is evaluated by computing eigenvalues of linearized Poincaré return map. By computing estimates of the basin of attraction (BoA) around fixed points corresponding to passive bounding gaits, it is shown that the proposed VPP controller enhances locomotion stability. The approach was tested in simulations with different perturbations including ground height variations up to 4.1 cm (20% of the nominal leg length). Finally, taking advantage of symmetries in the passively generated bounding gait leg motions on quadruped robots, the number of parameter variables of the controller was reduced. The methods and control laws proposed in this thesis are implemented in simulation models of the quadruped robot Minitaur.

Chapter 1

INTRODUCTION

1.1 Motivation and Objectives

Despite significant progress on wheeled robots, which resulted in fast and efficient mobile platforms, still a large portion of earth landmass is not accessible to such robots. Wheeled vehicles require a continuous path of support so that their wheels are always in contact with the ground when the vehicle is moving. Unlike wheeled vehicles, legged robots do not require continuous contact with the ground and this characteristic allows legged robots to accommodate extreme terrain conditions. As a result, legged robots are one of the alternative solutions to resolve limited mobility in an extreme terrain environment.

Since the first actively-balancing legged robot was introduced by Raibert and his collaborators [2], diverse of quadruped robots such as Scout II [30], Tekken [32], and BigDog [21, 22] have been developed. The majority of those robots implement heuristic controllers inspired by Raibert's original three part control method [2]. Various researches have been followed to obtain periodic motion of quadruped robots. Hybrid zero dynamics [42, 44], virtual constraints [63], and model predictive control methods [19, 50] were introduced to obtain asymptotically stable periodic motion of the system. However, improvements in control methods of quadruped robot also increased computational complexity to compute periodic solutions of the system which are desired trajectory of state.

Inspired from symmetry characteristics of passively generated bounding gait leg motions on quadruped robots [7, 62] and virtual pivot point observed in animal locomotion [8], our objective is to introduce a discrete-time control method that take advantage of the passive dynamics of the system.

1.2 Literature Review

In this section, we will review relevant literature for legged robot designs and methods for controlling their motion. Section 1.2.1 introduces passive and active-balancing walking models for biped robots. Section 1.2.2 provides quadruped robot control methods.

1.2.1 Passive and Active Control Methods of Legged Robots

The majority of legged robot research is about biped and quadruped robots. Biped robots can be divided into two categories as passive and active walkers. Recent interest in the passive walking model started with McGeer's research in the 1990s [14]. McGeer's four-link planar walker could perform periodic walking motions powered by gravity at 0.4 m/s (Fig. 1.1). This passive walker had locking knees to prevent collapse and circular feet to contact the ground.

Figure 1.1: McGeer's passive walker [20].

In the late 1990s, a three-dimensional passive walker was developed [64]. This walker had two arms and was able to move 0.5 m/s at a 3.1 degree downhill. These passive walkers showed self-stabilizing properties when walking with a fixed total energy. However, for practical control for biped robots, there should be external energy input toward the system [26].

Previous control method for biped robots used the zero moment point (ZMP) method. Early models of biped robots such as ASIMO [15, 16] and KHR series used a zero moment point control method to ensure stability while walking [23, 24, 25]. Since the zero moment point control method provides static stability guarantees, these robots moves at low speed, keeping at least one foot always on the ground; early versions of these systems could walk with velocities up to 0.5m/s. In the late 1990s, hybrid zero dynamics (HZD) with virtual constraint method was implemented to RABBIT by J. Grizzle [17]. By considering periodic locomotion behaviors, the virtual constraint [63] and hybrid zero dynamic methods successfully provided asymptotically periodic solutions, that were verified experimentally with RABBIT [43, 45, 46]. The HZD method has formed the basis for controlling compliant bipedal robots such as the planar biped MABEL [18]. This robot, 1.2 m tall and 32 kg in weight, reduced leg inertia by placing all actuators in the torso and reached 3.0 m/s speed. Another approach for control bipedal robot walking is to focus on controlling body posture [8]. Maus implemented virtual pendulum concept to biped. This control method created a Virtual Pivot Point (VPP), a virtual point on body where ground reaction forces directing, and control momentum force toward the body to make upright body posture.

1.2.2 Quadruped Robot Control Methods

A large variety of quadruped robots with different control methods were designed following Raibert's research toward dynamic legged robots in the 1980s, which provided a set of simple but effective physics-based laws for designing controllers for legged robots [1].

Quadrupedal robots share control methods with the bipedal robots case but has different approaches since in quadrupeds it is not necessary to maintain an upright posture of the torso. Early work by Raibert demonstrates an approach for the design of dynamic quadrupeds and their controllers. Hopping height is controlled by regulating energy input by pneumatic piston during stance phase. Forward velocity is controlled

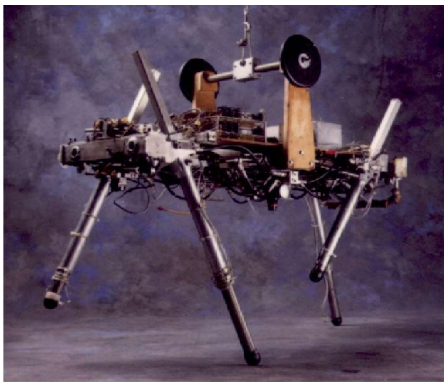

(a) Raibert's quadruped robot

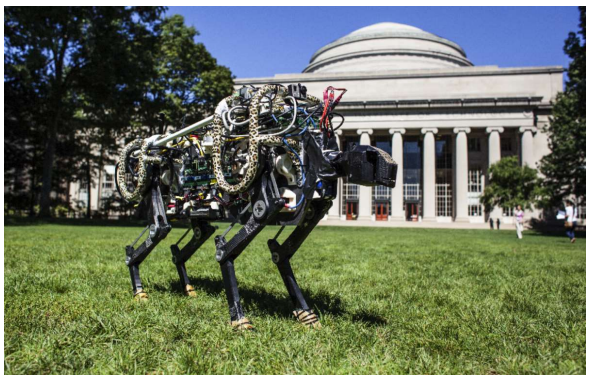

(b) Cheetah 2 [33]

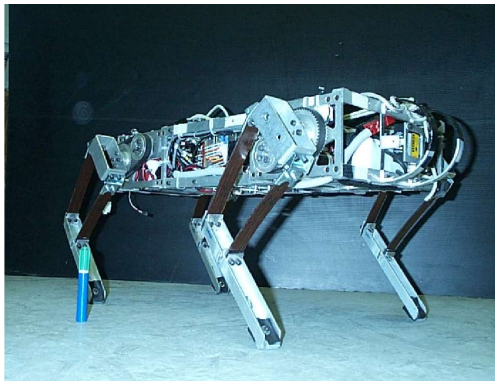

(c) Scout II

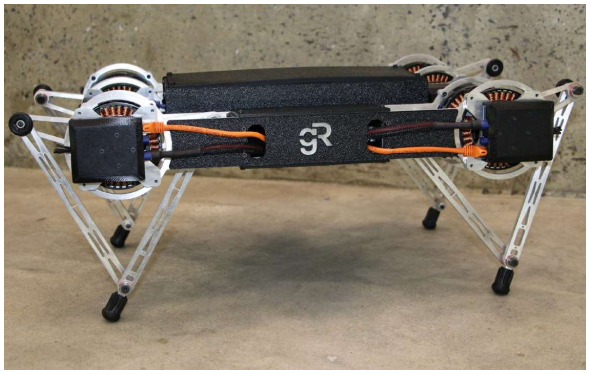

(d) Minitaur

Figure 1.2: Examples for quadruped robots. (a)Raibert's quadruped robot picture is retrieved from http://www.ai.mit.edu/projects/leglab/robots/quadruped/quadruped.html. (b) Cheethah 2 developed in MIT (c) Scout II picture is retrieved from http://research.me.udel.edu/ poulakas/index.html. (d) Minitaur picture is retrieved from KOD*LAB homepage, https://kodlab.seas.upenn.edu/robots/ghost-minitaur/

by foot placement at touchdown, and hip torque during stance phase is adjusted to control body attitude. Raibert's pioneering work on separating control problems in quadrupedal robots influenced later development of quadrupedal robot control methods. Scout II [30], BigDog [9, 10], KOLT [31], and Minitaur[40, 41] are subsequent quadrupedal robot designs that employed similar control methods to Raibert's approach. Scout II, the legs of which are composed of prismatic springs and controlled by a single hip joint actuator, successfully executed bounding and galloping motions by controlling touchdown angle of the leg during the flight phase and hip actuator torque during stance phase. The bounding gaits of Scout II demonstrated the relationship between touchdown and lift-off angles of the legs and stability of passive bounding gaits [29]. Unlike Scout II, the quadruped robot KOLT has two actuators for each leg which are both located in the hip joint and control the hip and knee angles. KOLT was able to realize pronking and trotting gait motion, and using Raibert's method to control its forward speed and its body pitch. BigDog also used Raibert's control method together with a virtual spring-mass model to move in rough terrain [10]. Similarly, the quadruped robot Minitaur also used Raibert's three part controller, but added a leg specialization control method for better performance in forward speed. In particular, by commanding a desired foot trajectory, it was possible to extend Minitaur's top forward speed to 2.9 m/s compared to 1.9 m/s, which was the maximum speed based on a straight forward implementation of Raibert's method [38].

As in bipedal robots, the method of hybrid zero dynamics [45] and model predictive control [49] can be used to control quadrupedal robot. Qu Cao implemented hybrid zero dynamics method to enforce virtual holonomic constraints on a quadrupedal bounding model with flexible torso [47, 48]. The symmetric relation between the touchdown and lift-off angles which was found in passive bounding with Scout II is also used to design a discrete-time controller that further enhances stability. Other control approaches for quadruped robots also exist; examples includes central pattern generators [52], impulse force control [33], and leg specialization control [38]. Central pattern generators (CPGs) have been implemented on Tekken resulting in walking over uneven

terrain [32]. Impulse control has been employed in [35] to stabilize the quadrupedal robot Cheetah 2. The controller essentially modifies the ground reaction force profiles so that these forces point to the system's center of mass. This allows Cheetah 2 to minimize body rotation and achieve separation of the control objectives so that the horizontal and vertical net forces become zero. Via impulse planning, Cheetah 2 can derive the desired ground reaction force profiles and realize them at its feet, resulting in bounding gaits with velocities varying from 0 m/s to 4.5 m/s [33].

1.2.3 Gait Motion Background

Quadrupedal gaits used for quadrupedal robot motion are mainly bounding, trotting, pronking, and galloping gait. These gaits are distinguished by four leg footfall sequence depending on contact with the ground. Fig 1.3 demonstrates the sequence motion of each leg for gait. In more detail,

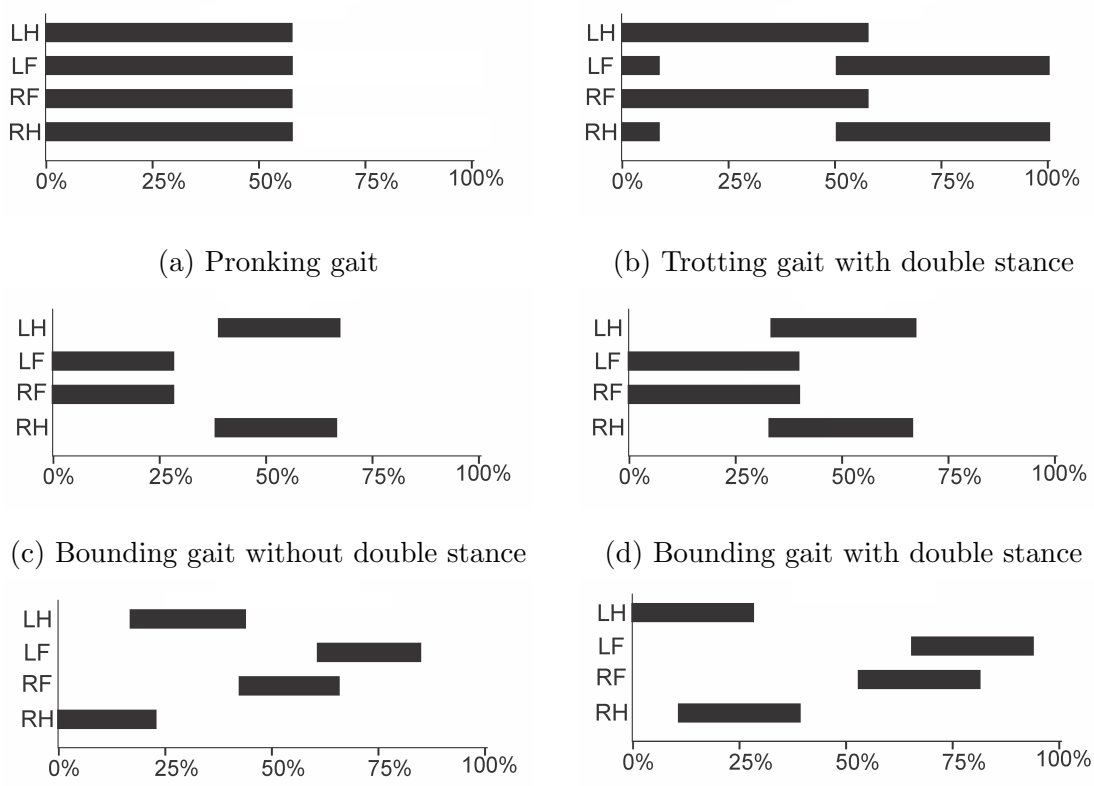

(a) Pronking gait

(b) Trotting gait with double stance

(c) Bounding gait without double stance

(d) Bounding gait with double stance

(e) Transverse galloping gait

(f) Rotary galloping gait

Figure 1.3: LP, LA, RA and RP in this plots indicate the left posterior, left anterior, right anterior, and right posterior legs. Bottom axis is percentage of one gait cycle. The black bar indicate that corresponding leg is touching the ground [51, 53].

During pronking, all four legs lift off and touchdown the ground at the same time resulting in low forward speeds. At moderate forward speeds, the trotting gait is employed; during this gait diagonal pairs of legs move simultaneously. At high speeds, bounding or galloping gait is typically employed. In bounding gait, the two front or back legs make a pair and move simultaneously. During bounding gait, there are four different phases, back (posterior) leg stance phase, front (anterior) leg stance phase, and two flight phases or double stance phases. When one pair of legs touches down to the ground before the other pair lifts off, a double stance emerges. It is not necessary to have a double stance phase to realize bounding. Flight phase starts when both leg

pairs take off from the ground and can be distinguished as gathered and extended flight phase depending on the motion of two leg pairs: in gathered, flight the two leg pairs point toward the center of the body while in extended flight they point away from the center; see Fig. 1.4. Galloping gait is a variation of bounding gait that is observed when legs in each pair, front or back, act with time difference. In animal locomotion, each gait pattern is used over a limited range of forward speed, transitioning between gait patterns to reduce the metabolic cost, or bone stresses [5, 13].

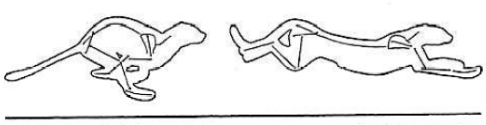

Figure 1.4: The sketch of gathered and extended flight phase by Hildebrand [51]

Raibert simplified quadrupedal gaits by combining pairs of legs that moves simultaneously in the sagittal plane [2, 3]. For pronking gait, all legs can be considered as one pair as they do the same motion. Therefore, pronking gait with virtual spring legs can be converted to simple model, namely the spring loaded inverted pendulum, which represents a virtual leg with stiffness four times stiffer than the physical legs. For the trotting gait, each of the diagonal pairs can be combined into one virtual leg. This combination results in effectively replacing trotting with bipedal walking. Regarding the bounding gait, it is still possible to reduce it to a virtual bipedal gait [27]. With this idea, Raibert realized successful transitions between trotting and pacing by controlling the touchdown angle of the legs with respect to the ground. Symmetry, well shown in animal movement [52], is an important issue for controlling periodic quadrupedal motion. Since symmetry motion ensures zero net force of system for one cycle of gait [11], this plays a key role in simplifying control for legged robots [4, 7]. For quadrupedal robots, the symmetry of motion may be shown in one stance phase or between posterior and anterior leg stance phases. The impulse planning method for Cheetah 2 also used symmetry by controlling touchdown angle and lift-off angle of leg in one stance phase [34, 36]. Symmetry in posterior and anterior leg stance phase was well shown in Scout

II bounding gait motion [12]. Relating the liftoff angle of one leg with the touchdown angle of the other, Scout II was able to conduct a periodic motion of bounding gait in simulation.

1.3 Summary of Contribution

In this thesis, we present a discrete-time controller for quadrupedal bounding gait motion in the sagittal plane. Specific contributions can be summarized as

- Proposing a controller that combine with the virtual pivot point concept with symmetry properties of the passive dynamics.
- Computing periodic orbits for the passive bounding gait system and for the proposed virtual pivot point controller at different forward speeds.
- Designing a discrete linear quadratic regulator to update the desired location of the VPP and the touchdown and liftoff angles.
- Reducing computational complexity of the proposed controller by utilizing symmetry to decrease the number of input parameter variables.
- Constructing safe transition map between periodic orbits with different forward speeds and verified by simulation results.

1.4 Organization of the Thesis

The remainder of this thesis is organized into four chapters.

Chapter 2 provides a description of the model and its bounding gait motion. 11-link quadrupedal robot simplified from Minitaur with 7 degree of freedoms is used for computing dynamic equations. Minitaur's leg have a symmetric five-bar shape, and we provide descriptions of the leg configuration as well as the relation between actuator torques and ground reaction forces [37, 39]. Under the assumption of very light weight legs, Minitaur's legs are converted to virtual spring leg for a simpler model and the relationship between the virtual spring leg and five bar leg is presented. Both constrained and unconstrained models are used to describe the stance and flight phase of bounding gait. In each case the dynamic equations are derived by using the Lagrange method. Description of phases for bounding gait and corresponding dynamic equation are explored.

Chapter 3 describes the proposed controller design, i.e. the Virtual Pivot Point (VPP) controller, for stabilizing bounding gait. Using a reduced parameter set, the modified dynamic equations for each phase are introduced. The proposed control method and dynamic equations using the Virtual Pivot Point concept is also derived. The method of Poincaré, for analyzing the stability and existence of periodic orbits, is introduced and adopted to study the dynamics for the bounding gait and evaluate stability properties of the system. A discrete Linear Quadratic Regulator (LQR) is derived and a method for estimating the basin of attraction is described. These results form the basis of the simulations conducted in Chapter 4.

Chapter 4 gives simulation results for quadrupedal bounding gait and consists of three parts. First, the stability properties of proposed controller are evaluated. Passive bounding gait motion is provided with repeating motion of each state variable, and the stability of this periodic motion is evaluated by the corresponding fixed point. Feedback controller is applied to enlarge basin of attraction around fixed point, and discrete linear quadratic regulator is used to compute feedback gain of the system. The VPP controller is applied to passive bounding gait. Performance of the VPP controller is evaluated by comparing simulation results with Minitaur undergoing unexpected ground height variations. Second, the number of input parameter variables is adjusted based on symmertry consideration to reduce complexity. Results of unexpected ground height variation test for the model with different control parameters are compared. Third, a safe transition map between periodic orbits with different forward speeds is described.

Chapter 5 concludes our thesis and deals with prospective on future directions relevant to this work.

Chapter 2

DYNAMIC MODELING

2.1 Notation and Assumption of the Model

In this thesis, we focus on bounding gait motion and develop a discrete time controller for enhancing stability. Since the two physical posterior legs move in an identical manner, we can capture their combined effect in a single virtual legs, similarly, the anterior physical legs can be represented as a virtual legs [3]. As a result, the sagittal plane model of Fig. 2.1 with 7 degrees of freedom will be used to study bounding.

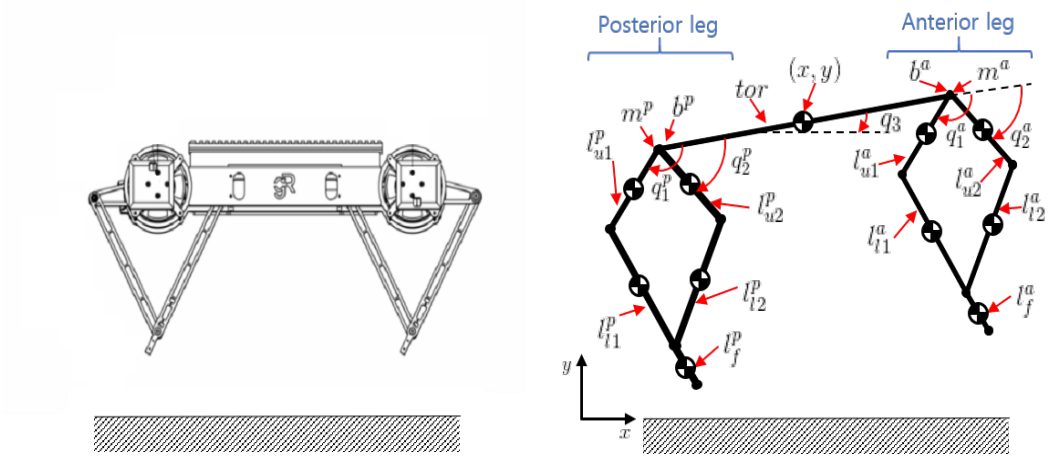

(a) Minitaur on sagittal plane with body, upper leg, and lower leg links.

(b) 11-link simplified sagittal model with configuration variables and notations.

Figure 2.1: (a) Minitaur design (retrieved from https://www.ghostrobotics.io/) and (b) Minitaur configuration in the sagittal plane

Seven configuration variables are described in Fig. 2.1b, which results in 14 state variables used to capture the motion of the model. The list of state variables and corresponding meaning are provided in Table 2.1.

Table 2.1: State variables and descriptions

State	Units	Description
q_1^p	deg (°)	1_{st} posterior leg angle from body
$\dot{q}_1^p$	deg/sec (°/s)	1_{st} posterior leg angular velocity
q_2^p	deg (°)	2_{nd} posterior leg angle from body
$\dot{q}_2^p$	deg/sec (°/s)	2_{nd} posterior leg angular velocity
q_1^a	deg (°)	1_{st} anterior leg angle from body
$\dot{q}_1^a$	deg/sec (°/s)	1_{st} anterior leg angular velocity
q_2^a	deg (°)	2_{nd} anterior leg angle from body
$\dot{q}_2^a$	deg/sec (°/s)	2_{nd} anterior leg angular velocity
q_3	deg (°)	body angle from fixed x-axis
$\dot{q}_3$	deg/sec (°/s)	body angular velocity
x	m	Horizontal location of body (center of mass)
$\dot{x}$	m/s	Horizontal velocity of body
y	m	Vertical location of body (center of mass)
$\dot{y}$	m/s	Vertical velocity of body

Each leg of Minitaur consists of five links which represent two thighs, two shins, and one foot part, see Fig. 2.1. We will denote the posterior leg "p", and the anterior leg with "a". Each leg has point feet at its end and the corresponding parameters for the inertia and geometric characteristics are presented in Table 2.2. As described in Fig. 2.1b, we use the notation "tor", "l_u", "l_l", and "l_f" for torso, upper leg, lower leg, and foot, respectively. Motor and motor bracket is denoted as "m" and "b".

Table 2.2: Model parameters of the quadruped robot Minitaur

Model Parameter	Units	Label	Value
Mass	kg	M_{tor}	4.6000
		M_{l_u}	$3.9200 * 10^{-2}$
		M_{l_l}	$3.9200 * 10^{-2}$
		M_{l_f}	$1.4137 * 10^{-2}$
		M_m	$1.8250 * 10^{-2}$
		M_b	$9.2809 * 10^{-2}$
Length	m	L_{tor}	$4.3440 * 10^{-1}$
		L_{l_u}	$1.0000 * 10^{-1}$
		L_{l_l}	$2.0000 * 10^{-1}$
		L_{l_f}	$2.5000 * 10^{-2}$
Inertia	$kg \cdot m^2$	I_{tor}	$5.4464 * 10^{-2}$
		I_{l_u}	$6.2745 * 10^{-5}$
		I_{l_l}	$1.6666 * 10^{-4}$
		I_{l_f}	$1.2723 * 10^{-6}$
		I_m	$1.0746 * 10^{-5}$
		I_b	$2.0119 * 10^{-4}$

The gravitational acceleration constant is assumed to be $9.8 m/s^2$ and the maximum allowable static friction coefficient is 0.9. Since one leg mass of Minitaur is approximately 3.7% of body mass, we assume that leg masses are negligible. Since leg masses are neglected, swing legs has no work during phases. Therefore, two flight phases of bounding gait motion is not distinguished with this assumption; see Fig. 2.2.

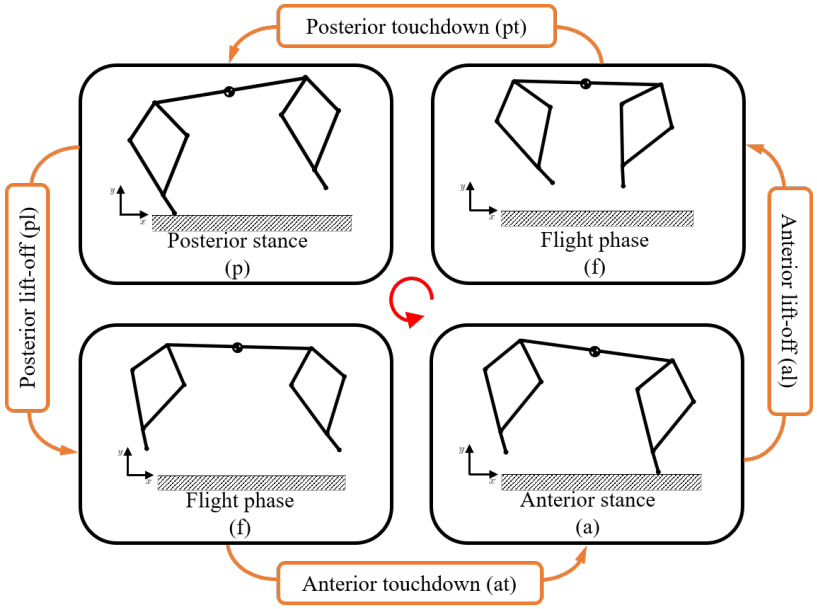

Figure 2.2: Bounding gait cycle without double stance phase

2.2 Leg Configuration

2.2.1 Link coordinate calculation

Motivated by the mechanics of animal running, in which the leg muscles show elastic behavior essentially moving link a spring leg to preserve and release energy [54], we will derive a controller so that the robot legs have similar energy recycling characteristics. Hence, the objective of the leg controller is to make the virtual leg operate as a spring; see Fig. 2.3. Since we assumed that leg masses are negligible, a straightforward calculation can be used to convert the force to actuator torques. We will denote virtual spring leg length as "l_v" and its angle with fixed x-axis as "θ_v" (Fig. 2.3).

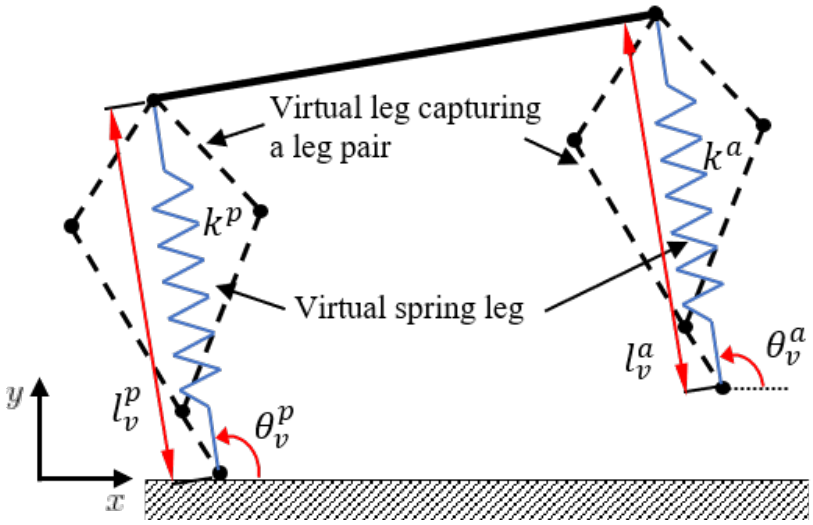

Figure 2.3: 11-link sagittal model with virtual spring leg. Virtual spring leg length is l_v, virtual spring leg angle is θ_v, and virtual spring leg stiffness is k. Parameter values used for virtual spring leg are described in Table 2.3.

Table 2.3: Description for parameter variables

Parameter	Description
θ^p	Angle of posterior virtual spring leg
θ^a	Angle of anterior virtual spring leg
l_v^p	Length of posterior virtual spring leg
l_v^a	Length of anterior virtual spring leg
k^p	Stiffness of posterior virtual spring leg
k^a	Stiffness of anterior virtual spring leg

Note that the position and angle of each link and virtual spring leg length and angle are described in Appendix A.

2.2.2 Force Calculation

As was mentioned above, a straightforward calculation can be used to convert the virtual spring leg force to actuator torques. To derive the force Jacobian matrix for

converting virtual spring leg force the the corresponding actuator torques, the virtual spring leg coordinates $v = (l_v^p, \theta_v^p, l_v^a, \theta_v^a)^\top$ should be derived by configuration coordinate variables $q = (q_1^p, q_2^p, q_1^a, q_2^a, q_3, x, y)^\top$.

$$\begin{aligned} v &= f(q) \\ \dot{v} &= \frac{\partial f(q)}{\partial q}\dot{q} = J(q)\dot{q} \\ J(q) &= \frac{\partial f(q)}{\partial q} \end{aligned} \tag{2.1}$$

Using (2.1), Jacobian matrix J(q_c) can be derived. The derived matrix $J(q)$ and the kinematics $f(q)$ are denoted in Appendix A. Since total work done by the system should be the same in both coordinates, we can derive relationship between forces in configuration coordinates and virtual spring leg coordinates. Let W_1 be the total work done by virtual spring leg, W_2 be the total work done by virtual leg, F be the virtual spring leg forces, τ be the actuator torques, and v be virtual leg coordinates as above. Then we can describe actuator torque set as

$$\begin{aligned} W_1 &= F_1\dot{v}_1 + F_2\dot{v}_2 + ... + F_4\dot{v}_4 = F^\top\dot{v}, \\ W_2 &= \tau_1\dot{q}_1 + \tau_2\dot{q}_2 + ... + \tau_7\dot{q}_7 = \tau^\top\dot{q}, \\ W_1 - W_2 &= 0 = F^\top\dot{v} - \tau^\top\dot{q} = (F^\top J(q) - \tau^\top)\dot{q}, \\ \tau &= J(q)^\top F, \end{aligned} \tag{2.2}$$

2.3 Dynamic Model Equation

As mentioned above, by assuming leg masses are negligible, bounding gait can be described by series of 3 different phases: the posterior leg stance phase, the anterior leg stance phase, and the flight phase, and 4 transitions: posterior leg touchdown and liftoff, and anterior leg touchdown and liftoff. Lagrange's method is used to derive the dynamic models for the sagittal-plane quadruped robot model of Fig. 2.1.

2.3.1 Flight Phase

When both legs are in the air, the system is in the flight phase. Since we assumed that leg masses are negligible, we can define dynamic variables ($q^f = (q_3, x, y)^\top$) and kinematic variables ($z^f = (q_1^p, q_2^p, q_1^a, q_2^a)^\top$) for the flight phase. Since flight phase ends when one leg touches the ground, kinematic variables are related to the configuration of legs and decide when flight phase ends. Dynamic variables are related to motion of the system and located in Q^f, which is 3 dimensional configuration space for flight phase. The total potential energy equation of the model can be described as

$$V(q^f) = M_{tor} g y, \tag{2.3}$$

where g is gravitational acceleration of $9.8 m/s^2$. The total kinetic energy equation of the model is

$$K(q^f, \dot{q}^f) = \frac{1}{2} M_{tor}((\dot{x})^2 + (\dot{y})^2) + \frac{1}{2} I_{tor}(\dot{q}_3)^2. \tag{2.4}$$

Given the expression of the potential energy by (2.3) and kinetic energy by (2.4), we can use Lagrange's method to derive the dynamic equations of the system. Let TQ^f be the 6 dimensional state space of the flight phase, the state vector of the flight phase, which is located in TQ^f, can be described as

$$x^f = [(q^f)^\top, (\dot{q}^f)^\top]^\top \in TQ^f. \tag{2.5}$$

The Lagrangian is a scalar valued function ($\mathcal{L} : TQ^f \to \mathbb{R}$) and defined as

$$\mathcal{L}(q^f, \dot{q}^f) = K(q^f, \dot{q}^f) - V(q^f) = \frac{1}{2} M_{tor}((\dot{x})^2 + (\dot{y})^2) + \frac{1}{2} I_{tor}(\dot{q}_3)^2 - M_{tor} g y. \tag{2.6}$$

Using (2.6) and Lagrange's equation

$$\frac{d}{dt}\frac{\partial \mathcal{L}}{\partial \dot{q}^f} - \frac{\partial \mathcal{L}}{\partial q^f} = \Gamma, \tag{2.7}$$

where Γ denotes forces and torques exerted to the system. The flight phase dynamic model can be derived as

$$D^f(q^f)\ddot{q}^f + C^f(q^f, \dot{q}^f)\dot{q}^f + G^f(q^f) = B^f(q^f)u^f, \tag{2.8}$$

where D^f is inertial matrix, C^f is Coriolis matrix, G^f is gravity vector, B^f can be derived by mapping motor torques to forces using the principle of virtual work, and $u^f = (u_1^p, u_2^p, u_1^a, u_2^a)$ is actuator torque which is composed of two motor torques for posterior leg and two motor torques of anterior leg. We can express (2.8) in state space form as

$$\dot{x}^f = f^f(x^f) + g^f(x^f)u^f, \tag{2.9}$$

where

$$f = \begin{bmatrix} \dot{q}^f \\ (D^f)^{-1}(-C^f\dot{q}^f - G^f) \end{bmatrix}, \qquad g = \begin{bmatrix} 0 \\ \dots \\ 0 \end{bmatrix}. \tag{2.10}$$

Since the leg mass and inertia are neglected, no forces and torques act on the system other than the gravitational force. Therefore, the equations of motion during the flight phase take the particularly simple form as

$$\dot{x}^f = \begin{bmatrix} \dot{q}^f \\ 0 \\ \vdots \\ 0 \\ -9.8 \end{bmatrix}. \tag{2.11}$$

2.3.2 Posterior Leg Stance Phase

When the posterior leg touches the ground during the flight phase, the posterior leg stance phase begins, see Fig. 2.2. Since one leg keep touching the ground during posterior leg stance phase, the model is constrained to the ground and has 5 degrees of freedom. Therefore, 5 coordinate variables, which are $q_1^p, q_2^p, q_1^a, q_2^a, q_3$ and described in Table 2.1, are needed to describe configuration of the posterior leg stance phase model. Since we assumed that leg masses are negligible, we can define dynamic variables ($q^p = (q_1^p, q_2^p, q_3)^\top$) and kinematic variables ($z^p = (q_1^a, q_2^a)^\top$) for the posterior leg stance

phase. Dynamic variables are located in Q^p, which is 3 dimensional configuration space for the posterior leg stance phase. Using dynamic variables, position of the torso ($p(q^p)$) can be expressed as

$$p_p(q^p) = (p_p^h(q^p), p_p^v(q^p)) = (x, y), \tag{2.12}$$

where $p_p^h(q^p)$ is horizontal position of torso and $p_p^v(q^p)$ is vertical position of torso. The total potential energy equation of the model can be described as

$$V(q^p) = M_{tor} g p_p^v(q^p), \tag{2.13}$$

where g is gravitational acceleration of $9.8 m/s^2$. The total kinetic energy equation of the model is

$$K(q^p, \dot{q}^p) = \frac{1}{2} M_{tor}((\dot{p}_h^p(q^p))^2 + (\dot{p}_v^p(q^p))^2) + \frac{1}{2} I_{tor}(\dot{q}_3)^2. \tag{2.14}$$

Given the expression of the potential energy by (2.13) and kinetic energy by (2.14), we can use Lagrange's method to derive the dynamic equations of the system. Let TQ^p be the 6 dimensional state space of the posterior leg stance phase, the state vector, which is located in TQ^p, can be described as

$$x^p = [(q^p)^\top, (\dot{q}^p)^\top]^\top \in TQ^p. \tag{2.15}$$

The Lagrangian is a scalar valued function ($\mathcal{L} : TQ^p \to \mathbb{R}$) and defined as

$$\mathcal{L}(q^p, \dot{q}^p) = K(q^p, \dot{q}^p) - V(q^p) = \frac{1}{2} M_{tor}((\dot{p}_h^p(q^p))^2 + (\dot{p}_v^p(q^p))^2) + \frac{1}{2} I_{tor}(\dot{q}_3)^2 - M_{tor} g p_p^v(q^p). \tag{2.16}$$

Using (2.16) and Lagrange's equation

$$\frac{d}{dt}\frac{\partial \mathcal{L}}{\partial \dot{q}^p} - \frac{\partial \mathcal{L}}{\partial q^p} = \Gamma, \tag{2.17}$$

where Γ denotes forces and torques exerted to the system. The posterior leg stance phase dynamic model can be derived as

$$D^p(q^p)\ddot{q}^p + C^p(q^p, \dot{q}^p)\dot{q}^p + G^p(q^p) = B^p(q^p)u^p, \tag{2.18}$$

where D^p is inertial matrix, C^p is Coriolis matrix, G^p is gravity vector, B^p can be derived by mapping motor torques to forces using the principle of virtual work, and $u^p = (u_1^p, u_2^p, u_1^a, u_2^a)$ is actuator torque which is composed of two motor torques for posterior leg and two motor torques of anterior leg. We can express (2.18) in state space form as

$$\dot{x}^p = f^p(x^p) + g^p(x^p)u^p, \tag{2.19}$$

where

$$f = \begin{bmatrix} \dot{q}^p \\ (D^p)^{-1}(-C^p\dot{q}^p - G^p) \end{bmatrix}, \qquad g = \begin{bmatrix} 0 \\ B^p(q^p) \end{bmatrix}. \tag{2.20}$$

2.3.3 Anterior Leg Stance Phase

When the anterior leg touches the ground during the flight phase, the anterior leg stance phase begins, see Fig. 2.2. Since one leg keep touching the ground during anterior leg stance phase, the model is constrained to the ground and has 5 degrees of freedom. Therefore, 5 coordinate variables, which are $q_1^p, q_2^p, q_1^a, q_2^a, q_3$ and described in Table 2.1, are needed to describe configuration of the anterior leg stance phase model. Since we assumed that leg masses are negligible, we can define dynamic variables ($q^p = (q_1^a, q_2^a, q_3)^\top$) and kinematic variables ($z^p = (q_1^p, q_2^p)^\top$) for the anterior leg stance phase. Dynamic variables are located in Q^a, which is 3 dimensional configuration space for the anterior leg stance phase. Using dynamic variables, position of the torso ($p(q^a)$) can be expressed as

$$p_a(q^a) = (p_a^h(q^a), p_a^v(q^a)) = (x, y), \tag{2.21}$$

where $p_a^h(q^a)$ is horizontal position of torso and $p_a^v(q^a)$ is vertical position of torso. The total potential energy equation of the model can be described as

$$V(q^a) = M_{tor} g p_a^v(q^a), \tag{2.22}$$

where g is gravitational acceleration of $9.8m/s^2$. The total kinetic energy equation of the model is

$$K(q^a, \dot{q}^a) = \frac{1}{2} M_{tor}((\dot{p}_h^a(q^a))^2 + (\dot{p}_v^a(q^a))^2) + \frac{1}{2} I_{tor}(\dot{q}_3)^2. \tag{2.23}$$

Given the expression of the potential energy by (2.22) and kinetic energy by (2.23), we can use Lagrange's method to derive the dynamic equations of the system. Let TQ^a be the 6 dimensional state space of the anterior leg stance phase, the state vector, which is located in TQ^a, can be described as

$$x^a = [(q^a)^\top, (\dot{q}^a)^\top]^\top \in TQ^a. \tag{2.24}$$

The Lagrangian is a scalar valued function ($\mathcal{L} : TQ^a \to \mathbb{R}$) and defined as

$$\mathcal{L}(q^a, \dot{q}^a) = K(q^a, \dot{q}^a) - V(q^a) = \frac{1}{2} M_{tor}((\dot{p}_h^a(q^a))^2 + (\dot{p}_v^a(q^a))^2) + \frac{1}{2} I_{tor}(\dot{q}_3)^2 - M_{tor} g p_a^v(q^a). \tag{2.25}$$

Using (2.25) and Lagrange's equation

$$\frac{d}{dt}\frac{\partial \mathcal{L}}{\partial \dot{q}^a} - \frac{\partial \mathcal{L}}{\partial q^a} = \Gamma, \tag{2.26}$$

where Γ denotes forces and torques exerted to the system. The anterior leg stance phase dynamic model can be derived as

$$D^a(q^a)\ddot{q}^a + C^a(q^a, \dot{q}^a)\dot{q}^a + G^a(q^a) = B^a(q^a)u^a, \tag{2.27}$$

where D^a is inertial matrix, C^a is Coriolis matrix, G^a is gravity vector, B^a can be derived by mapping motor torques to forces using the principle of virtual work, and $u^a = (u_1^p, u_2^p, u_1^a, u_2^a)$ is actuator torque which is composed of two motor torques for posterior leg and two motor torques of anterior leg. We can express (2.27) in state space form as

$$\dot{x}^a = f^a(x^a) + g^a(x^a)u^a, \tag{2.28}$$

where

$$f = \begin{bmatrix} \dot{q}^a \\ (D^a)^{-1}(-C^a\dot{q}^a - G^a) \end{bmatrix}, \quad g = \begin{bmatrix} 0 \\ B^a(q^a) \end{bmatrix}. \tag{2.29}$$

2.3.4 Transitions

When stance leg lift off from the ground during stance phases or one leg touches the ground during the flight phase, current phase is ended and transition to the next phase begins. As mentioned above, 4 transitions, which are posterior leg touchdown and liftoff, and anterior leg touchdown and liftoff, exist during bounding gait motion, see Fig. 2.2. Since we assumed that leg masses are negligible, transition will directly convert current state to the next state.

2.3.4.1 Posterior Leg Lift-off

When posterior leg lifts off the ground during the posterior leg stance phase, state is located in posterior leg lift-off switching surface (S_{pl}). After posterior leg lift-off transition, flight phase begins. This switching surface is subset of state space of the posterior leg stance phase (TQ^p). As we described position of torso by state of posterior leg stance phase in (2.12), we can describe state variables of the flight phase by state of the posterior leg stance phase as

$$\begin{aligned} q_3^+ &= q_3^- \\ (x^+, y^+) &= p_p(q^{p-}) \\ \dot{q}_3^+ &= \dot{q}_3^- \\ (\dot{x}^+, \dot{y}^+)^\top &= (\frac{\partial p_p(q^p)}{\partial q^p}\dot{q}^{p-})^\top \end{aligned} \tag{2.30}$$

where $q^p = (q_1^p, q_2^p, q_3)^\top$ is dynamic variable of the posterior leg stance phase. (2.30) can be expressed as

$$x^{f+} = \triangle_{pl}(x^{p-}), \qquad x^p \in S_{pl}, \tag{2.31}$$

2.3.4.2 Anterior Leg Lift-off

When anterior leg lifts off the ground during the anterior leg stance phase, state is located in anterior leg lift-off switching surface (S_{al}). After anterior leg lift-off transition, flight phase begins. This switching surface is subset of state space of the

anterior leg stance phase (TQ^a). As we described position of torso by state of anterior leg stance phase in (2.21), we can describe state variables of the flight phase by state of the anterior leg stance phase as

$$\begin{aligned} q_3^+ &= q_3^- \\ (x^+, y^+) &= p_a(q^{a-}) \\ \dot{q}_3^+ &= \dot{q}_3^- \\ (\dot{x}^+, \dot{y}^+)^\top &= (\frac{\partial p_a(q^a)}{\partial q^a}\dot{q}^{a-})^\top \end{aligned} \tag{2.32}$$

where $q^a = (q_1^a, q_2^a, q_3)^\top$ is dynamic variable of the anterior leg stance phase. (2.32) can be expressed as

$$x^{f+} = \triangle_{al}(x^{a-}), \qquad x^a \in S_{al}, \tag{2.33}$$

2.3.4.3 Posterior Leg Touchdown

When posterior leg touches the ground during the flight phase, state is located in posterior leg touchdown switching surface (S_{pt}). After posterior leg touchdown transition, the posterior leg stance phase begins. This switching surface is subset of state space of the flight phase (TQ^f). As we described position of torso by state of posterior leg stance phase in (2.12), we can describe state variables of the posterior leg stance phase by state of the flight phase as

$$\begin{aligned} q_3^+ &= q_3^- \\ (q_1^{p+}, q_2^{p+}) &= p_p^{-1}(q^{f-}) \\ \dot{q}_3^+ &= \dot{q}_3^- \\ (\dot{q}_1^{p+}, \dot{q}_2^{p+})^\top &= (\frac{\partial p_p^{-1}(q^f)}{\partial q^f}\dot{q}^{f-})^\top \end{aligned} \tag{2.34}$$

where $q^f = (q_3, x, y)^\top$ is dynamic variable of the flight phase. (2.34) can be expressed as

$$x^{p+} = \triangle_{pt}(x^{f-}), \qquad x^f \in S_{pt}, \tag{2.35}$$

2.3.4.4 Anterior Leg Touchdown

When anterior leg touches the ground during the flight phase, state is located in anterior leg touchdown switching surface (S_{at}). After anterior leg touchdown transition, the anterior leg stance phase begins. This switching surface is subset of state space of the flight phase (TQ^f). As we described position of torso by state of anterior leg stance phase in (2.21), we can describe state variables of the anterior leg stance phase by state of the flight phase as

$$\begin{aligned} q_3^+ &= q_3^- \\ (q_1^{a+}, q_2^{a+}) &= p_a^{-1}(q^{f-}) \\ \dot{q}_3^+ &= \dot{q}_3^- \\ (\dot{q}_1^{a+}, \dot{q}_2^{a+})^\top &= (\frac{\partial p_a^{-1}(q^f)}{\partial q^f}\dot{q}^{f-})^\top \end{aligned} \tag{2.36}$$

where $q^f = (q_3, x, y)^\top$ is dynamic variable of the flight phase. (2.34) can be expressed as

$$x^{a+} = \triangle_{at}(x^{f-}), \qquad x^f \in S_{at}, \tag{2.37}$$

2.3.5 Summary of Dynamic Equations

As we derive dynamic equations for 3 different phases and 4 transitions, dynamic equations for one bounding gait cycle can be summarized as

$$
\begin{aligned}
\sum\nolimits_{p} : &\begin{cases} \dot{x}^{p} &= f^{p}(x^{p}) + g^{p}(x^{p})u^{p}, & x^{p} \notin S_{pl} \\ x^{f+} &= \triangle_{pl}(x^{p-}), & x^{p} \in S_{pl} \end{cases}, \\
\sum\nolimits_{f1} : &\begin{cases} \dot{x}^{f} &= f^{f}(x^{f}) + g^{f}(x^{f})u^{f}, & x^{f} \notin S_{at} \\ x^{a+} &= \triangle_{at}(x^{f-}), & x^{f} \in S_{at} \end{cases}, \\
\sum\nolimits_{a} : &\begin{cases} \dot{x}^{a} &= f^{a}(x^{a}) + g^{a}(x^{a})u^{a}, & x^{a} \notin S_{al} \\ x^{f+} &= \triangle_{al}(x^{a-}), & x^{a} \in S_{al} \end{cases}, \\
\sum\nolimits_{f2} : &\begin{cases} \dot{x}^{f} &= f^{f}(x^{f}) + g^{f}(x^{f})u^{f}, & x^{f} \notin S_{pt} \\ x^{p+} &= \triangle_{pt}(x^{f-}), & x^{f} \in S_{pt} \end{cases}.
\end{aligned}
\tag{2.38}
$$

Chapter 3

CONTROLLER DESIGN

In this chapter, we will denote the description for a new discrete-time control method and method to evaluate stability of the system. Quadruped bounding gait does repeating motion when state of the system is in fixed point. Therefore, we can interpret this repeating motion as periodic solution of the system.

3.1 Passive Bounding Gait

3.1.1 Dynamic Equation for Passive Bounding Gait

We will denote quadruped bounding gait model with virtual spring leg as passive bounding gait since there exists no additional input to the system except virtual spring leg forces during passive bounding gait motion. Since no forces are exerted to the passive bounding gait model, inputs of dynamic equations (u^f,u^p, and u^a) derived in Chapter 2 can be described by an input parameter variable set (α) and state.

3.1.1.1 Stance Phase

During posterior stance phase, parameter variables such as touchdown angle and length of anterior virtual spring leg (l_v^a, θ_{td}^a) and state variables related to torso ($q_3, \dot{q}_3$) can describe state variables related to anterior virtual leg ($q_1^a, q_2^a, \dot{q}_1^a, \dot{q}_2^a$). Input parameter set for posterior stance phase (α^p) is

$$\alpha^p = [k^p, l_v^a, \theta_{td}^a]^\top, \tag{3.1}$$

where k^p is a virtual spring stiffness of posterior leg, l_v^a is virtual spring leg length of anterior leg, and θ_{td}^a is touchdown angle of virtual anterior spring leg. With state

(x^p) and input parameter set (α^p) for posterior stance phase, we can define input (u^p), which is posterior leg actuator torque, as a function of x^p and α^p.

$$u^p = \Gamma_p(x^p, \alpha^p), \tag{3.2}$$

where Γ_p is function describing input (u^p) by state (x^p) and parameter values (α^p) for the posterior leg stance phase. Using 3.1 and 3.2, dynamic equation for posterior stance phase (2.11) can be modified as

$$\begin{aligned} \dot{x}^p &= f^p(x^p) + g^p(x^p)\Gamma_p(x^p, \alpha^p), \\ \dot{x}^p &= f^p_{cl}(x^p, \alpha^p), \end{aligned} \tag{3.3}$$

where f^p_{cl} is modified closed loop function. For the anterior leg stance phase, we can use similar method to modify dynamic equation of anterior stance phase. Input parameter set for anterior stance phase (α^a) is

$$\alpha^a = [k^a, l^p_v, \theta^p_{td}]^\top, \tag{3.4}$$

where notations are described in Table 2.3. The parameter k^a is a virtual spring stiffness of anterior leg, l^p_v is virtual spring leg length of posterior leg, and θ^p_{td} is touchdown angle of virtual posterior spring leg. With reduced state (x^a) and input parameter set (α^p) for anterior stance phase, we can define input (u^a), which is anterior leg actuator torque, as a function of x^a and α^a.

$$u^a = \Gamma_a(x^a, \alpha^a), \tag{3.5}$$

where h^a is function describing input (u^a) by state (x^a) and parameter values (α^a) for anterior leg stance phase. Using 3.4 and 3.5, dynamic equation for anterior stance phase can be modified as

$$\begin{aligned} \dot{x}^a &= f^a(x^a) + g^a(x^a)\Gamma_a(x^a, \alpha^a), \\ \dot{x}^a &= f^a_{cl}(x^a, \alpha^a), \end{aligned} \tag{3.6}$$

where f_{cl}^{a} is modified closed loop function.

3.1.1.2 Flight Phase

During the flight phase, we can describe both legs using reduced state (x^f) and input parameter variables for both legs ($l_v^p, \theta_{td}^p, l_v^a$, and θ_{td}^a). Input parameter set for flight phase (α^f) is

$$\alpha^f = [k^p, k^a, l_v^p, \theta_{td}^p, l_v^a, \theta_{td}^a]^\top, \tag{3.7}$$

where notations are described in Table 2.3. With state (x^f) and input parameter set (α^f) for the flight phase, we can define input (u^f), which is actuator torque, as a function of x^f and α^f.

$$u^f = \Gamma_f(x^f, \alpha^f), \tag{3.8}$$

where Γ_f is function describing input (u^f) by state (x^f) and parameter values (α^f) for the flight phase. Using 3.7 and 3.8, dynamic equation for the flight phase can be modified as

$$\begin{aligned} \dot{x}^f &= f^f(x^f) + g^f(x^f)\Gamma_f(x^f, \alpha^f), \\ \dot{x}^f &= f_{cl}^f(x^f, \alpha^f), \end{aligned} \tag{3.9}$$

where f_{cl}^f is modified closed loop functions.

3.1.1.3 Full Dynamic Equation of Bounding Gait

Dynamic equation for full cycle of bounding gait motion described in (2.38) can be described as

$$
\begin{aligned}
\sum\nolimits_{p} : &\begin{cases} \dot{x}^{p} &= f_{cl}^{p}(x^{p}, \alpha^{p}), & x^{p} \notin S_{pl} \\ x^{f+} &= \triangle_{pl}(x^{p-}), & x^{p} \in S_{pl} \end{cases}, \\
\sum\nolimits_{f1} : &\begin{cases} \dot{x}^{f} &= f_{cl}^{f}(x^{f}, \alpha^{f}), & x^{f} \notin S_{at} \\ x^{a+} &= \triangle_{at}(x^{f-}), & x^{f} \in S_{at} \end{cases}, \\
\sum\nolimits_{a} : &\begin{cases} \dot{x}^{a} &= f_{cl}^{a}(x^{a}, \alpha^{a}), & x^{a} \notin S_{al} \\ x^{f+} &= \triangle_{al}(x^{a-}), & x^{a} \in S_{al} \end{cases}, \\
\sum\nolimits_{f2} : &\begin{cases} \dot{x}^{f} &= f_{cl}^{f}(x^{f}, \alpha^{f}), & x^{f} \notin S_{pt} \\ x^{p+} &= \triangle_{pt}(x^{f-}), & x^{f} \in S_{pt} \end{cases}.
\end{aligned}
\tag{3.10}
$$

3.2 Virtual Pivot Point Control Method

Inspired by Virtual Pendulum (VP) concept found in animal locomotion [8] and H.-M. Maus's research about Virtual Pivot Point (VPP) controller for biped model (Fig. 3.1a), the proposed control method will control its virtual pivot point locations (Fig. 3.1b). Maus used VP concept to enhance stability of biped robot by placing virtual pivot point, which is made by ground reaction force vectors, above center of mass of torso which makes body act like virtual pendulum. In our proposed controller, by changing the virtual pivot point of leg, amount and direction of force applied toward body can be modified during stance phases.

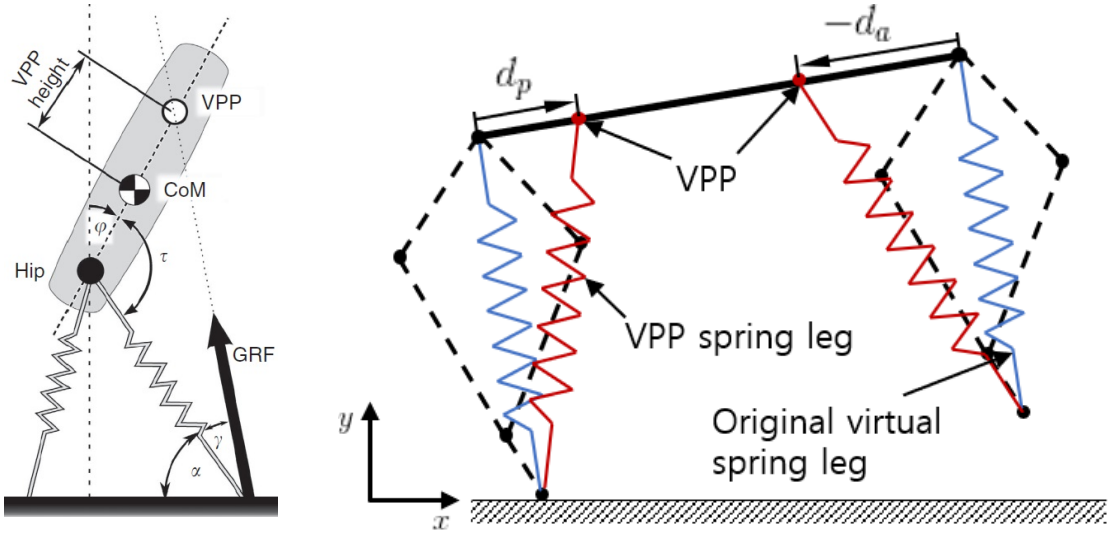

(a) The virtual pivot point controller made by H.-M. Maus[8]

(b) Minitaur model configuration with its leg (dash line), original virtual spring leg (blue line) and modified pivot point virtual spring leg (red line)

Figure 3.1: VPP concept controller for (a)biped and (b)quadruped

In Fig. 3.1, blue spring line indicates a virtual spring leg of passive bounding gait and red spring line is modified virtual spring leg by VPP controller. Parameter d_p and d_a are distances from posterior and anterior hip joint to virtual pivot point respectively, see Fig. 3.1b.

3.2.1 Dynamic Equation for VPP Controlled Bounding Gait

To apply VPP controller to the system, parameter variables (d_p and d_a) for VPP controller should be added to input parameter set. Since flight phases have no virtual spring force acting toward hip joints, only input parameter set for posterior and anterior leg stance phases will be changed. Modified input parameter variable sets for posterior (α^p_{vpp}) and anterior leg stance phases (α^a_{vpp}) are

$$\begin{aligned} \alpha^p_{vpp} &= [k^p, d^p, l^a_v, \theta^a_{td}]^\top, \\ \alpha^a_{vpp} &= [k^a, d^a, l^p_v, \theta^p_{td}]^\top, \end{aligned} \tag{3.11}$$

where d^p is distance from posterior hip joint to virtual pivot point used for posterior leg, and d^a is distance from anterior leg hip joint to virtual pivot point of anterior leg along mid-line of body. Similar to the passive bounding gait case, input of VPP controlled posterior leg stance phase, which is posterior leg actuator torque (u^p_{vpp}), can be described as a function of state (x^p) and input parameter set (α^p_{vpp}). For VPP controlled anterior leg stance phase, similar approach to VPP controlled posterior leg stance phase is used. Input for stance phases are

$$\begin{aligned} u^p_{vpp} &= \Gamma^{vpp}_p(x^p, \alpha^p_{vpp}), \\ u^a_{vpp} &= \Gamma^{vpp}_a(x^a, \alpha^a_{vpp}), \end{aligned} \tag{3.12}$$

where Γ^{vpp}_p is function describing input (u^p_{vpp}) by state (x^p) and modified parameter variable set (α^p_{vpp}) for VPP controlled posterior leg stance phase, and Γ^{vpp}_a is function describing input (u^a_{vpp}) by state (x^a) and modified parameter variable set (α^a_{vpp}) for VPP controlled anterior leg stance phase. Dynamic equation for full cycle of VPP controlled bounding gait can be described with 4 modified continuous phases ($\sum^{vpp}_p$,$\sum^{vpp}_{f1}$, $\sum^{vpp}_a$, and $\sum^{vpp}_{f2}$).

$$\begin{aligned} \sum\nolimits^{vpp}_p : \begin{cases} \dot{x}^p &= f^p_{vpp}(x^p, \alpha^p_{vpp}), & x^p \notin S_{pl} \\ x^{f+} &= \triangle_{pl}(x^{p-}), & x^p \in S_{pl} \end{cases}, \\ \sum\nolimits_{f1} : \begin{cases} \dot{x}^f &= f^f(x^f) + g^f(x^f)u^f, & x^f \notin S_{at} \\ x^{a+} &= \triangle_{at}(x^{f-}), & x^f \in S_{at} \end{cases}, \\ \sum\nolimits^{vpp}_a : \begin{cases} \dot{x}^a &= f^a_{vpp}(x^a, \alpha^a_{vpp}), & x^a \notin S_{al} \\ x^{f+} &= \triangle_{al}(x^{a-}), & x^a \in S_{al} \end{cases}, \\ \sum\nolimits_{f2} : \begin{cases} \dot{x}^f &= f^f(x^f) + g^f(x^f)u^f, & x^f \notin S_{pt} \\ x^{p+} &= \triangle_{pt}(x^{f-}), & x^f \in S_{pt} \end{cases}, \end{aligned} \tag{3.13}$$

where dynamic equations for the flight phases are not changed.

3.3 Periodic Orbit

When the system is repeating its bounding gait motion, state variables of the system makes its trajectory as periodic orbit during this bounding gait motion [55]. In this quadruped model, except horizontal location of torso (x), state variables $(q_1^p, q_2^p, q_1^a, q_2^a, q3, y)$ will make their trajectory as periodic orbit during repeating bounding gait motion of the system. From dynamic equations of VPP controlled bounding gait in 3.13, we will combine those dynamic equations to one equation with full input parameter set (α_{total}) which contains all parameter variables used for previous input parameter sets (α_{vpp}^p, α_{vpp}^a, and α^f). The combined dynamic equation of the system is

$$\dot{x}^p = F(x^p, \alpha_{total}), \tag{3.14}$$

where F is a combined function and α_{total} includes all parameter variables used in other input variable sets. let $\phi(t) : [t_0, t_f] \to \mathcal{X}, t_f \in \mathbb{R} \cup \{\infty\}$, $\mathcal{X}$ is state space, to be a periodic orbit and solution of 3.14. Then there exists a finite positive T for any $t \in [t_o, t_f]$ satisfying

$$\phi(t + T) = \phi(t). \tag{3.15}$$

Therefore, the periodic orbit $\mathcal{O} \subset \mathcal{X}, \mathcal{O} = \{\phi(t) | t \geq t_0\}$ can be defined. The periodic orbit $\mathcal{O}$ can be said stable in the sense of Lyapunov if $\forall \epsilon > 0$, there $\exists \mathcal{V}$ (where $\mathcal{V}$ is open neighborhood of $\mathcal{O}$) such that $\forall p \in \mathcal{V}$, $\exists \psi$ (where $\psi : [0, \infty) \to \mathcal{X}$ is solution of 3.14) which satisfies

$$d(\psi, \mathcal{O}) < \epsilon, \ \ where \ \ \psi(0) = p, t \geq 0, \tag{3.16}$$

where $d(\psi, \mathcal{O})$ is the closest distance from ψ to $\mathcal{O}$. In addition, $\mathcal{O}$ is attractive when $\exists \psi : [0, \infty) \to \mathcal{X}$ which satisfies

$$d(\psi, \mathcal{O}) \to 0, \ as \ t \to 0 \ \ for \ \ \psi(0) = p. \tag{3.17}$$

Therefore, $\mathcal{O}$ is asymptotically stable in the sense of Lyapunov when it is both attractive and stable. To determine stability of periodic orbit, the Poincaré return map method is used.

3.3.1 Poincaré Map

Through the Poincaré return map method, we can transform our problem to find periodic orbit from the dynamic equation (3.14) to find an equilibrium point from discrete-time system. Therefore, the existence of periodic orbit in continuous-time dynamic equation corresponds to the existence of equilibrium point is discrete-time system [55]. If the Poincaré return map is asymptotically stable around its fixed point, then periodic orbit is also asymptotically stable. To defined the Poincaré return map of the system, we need to choose the Poincaré section, a subset of state space, which should transversal to periodic orbit. The transversality means that the orbit starting from the Poincaré section should cross and not parallel to orbit after one time period. To reduce dimension of state space and considering non-repeating state variable "x", we should choose the Poincaré section in constrained case. We will choose the Poincaré section to the end of posterior leg stance phase in this thesis. From 3.14 the Poincaré return map in the discrete-time system is defined as

$$x[k+1] = P(x[k], \alpha[k]), \tag{3.18}$$

where k is positive number and represents number of iterations, x[k] is state in k_{th} iteration, and $\alpha[k]$ is input parameter set of k_{th} iteration.

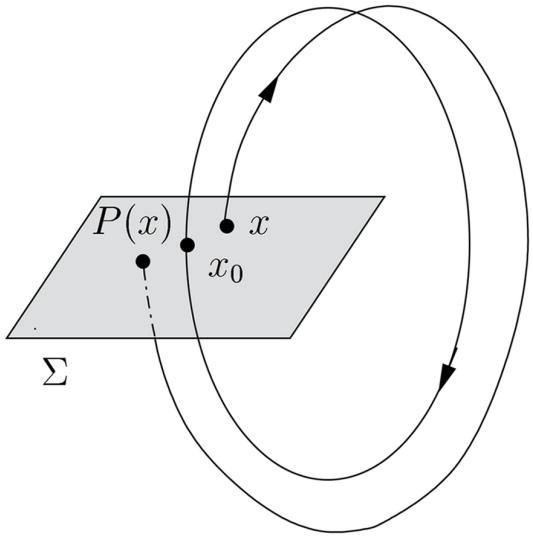

Figure 3.2: Poincaré return map with Poincaré section $\sum$ with fixed point x_0[6]

Using 3.17 we can simply find the periodic orbit of dynamic system to search equilibrium point, i.e.,

$$x - P(x, \alpha) = 0 \tag{3.19}$$

It is obvious that x is equilibrium point and returns to same value after one period. To determine local stability of the Poincaré return map around fixed point, we will linearize 3.17 at the fixed point. Let p to be fixed point of the Poincaré return map and parameter variables have fixed values, the linearized Poincaré return map is

$$\triangle x[k+1] = A \triangle x[k], \tag{3.20}$$

where $\triangle x[k] = x[k] - p$ and $A = \frac{dP}{dx}|_{x=p}$. Let $v = x - p, v[0] = v_0$, which is eigenvector of matrix A,

$$v[k+1] = A^{k+1} v[0] = \lambda^{k+1} v[0], \tag{3.21}$$

where λ is eigenvalue set of A. Therefore, when all eigenvalues are located in unit circle ($|\lambda| < 1$), the corresponding fixed point is locally exponentially stable and the Poincaré return map converges to fixed point as iteration proceed [55, 56]. However,

this stability analysis is limited to local stability around a fixed point. Therefore, we need to estimate basin of attraction (BoA) of this fixed point which is region where the system converges to fixed point. The basin of attraction of a locally asymptotically stable fixed point is an invariant set that all trajectories starting inside of this set will finally converge to the fixed point.

3.4 Basin of Attraction Estimation

To ensure convexity of estimating BoA, we will use sum of square (SoS) method to estimate basin of attraction of the fixed point. To use the sum of square method, we will transform the Poincaré return map to polynomial form by 2_{nd} Taylor expansion. With polynomial equation form of the Poincaré return map computed by 2_{nd} Taylor expansion, Lyapunov function (V($\triangle x[k]$)) candidate can be computed. Basin of attraction is then estimated by the area where V($\triangle x[k]$) is SoS (where V($\triangle x[k]$) $\geq \rho$) and -dV($\triangle x[k]$) is also SoS (where dV($\triangle x[k]$) = V($\triangle x[k+1]$)-V($\triangle x[k]$) $\leq -\epsilon \triangle x^T[k] \triangle x[k]$ (where ϵ is small positive scalar, $\rho \geq 0$). These two conditions mean the area where the Lyapunov function (V($\triangle x[k]$) is positive and decreases as iteration continues [57]. Therefore, the Lyapunov function will converge to zero when state goes to fixed point as iteration continues. To ensure above conditions, we will introduce function s($\triangle x[k]$) as a SoS function (where s($\triangle x[k]$) ≥ 0) and conditions are modified as

$$\{\triangle x[k]| - (dV(\triangle x[k]) + \epsilon \triangle x^T[k] \triangle x[k]) - s(\triangle x[k])(\rho - V(\triangle x[k]))\} \geq 0$$

$$then,$$

$$\{\triangle x[k]|V(\triangle x[k]) - \rho \geq 0\} \subset \{\triangle x[k]| - (dV(\triangle x[k]) + \epsilon \triangle x^T[k] \triangle x[k]) \geq 0\}. \tag{3.22}$$

To make a more accurate estimation for basin of attraction, we will find maximum ρ from given $V(\triangle x[k]), s(\triangle x[k]), \epsilon$. Then, we will conduct iteration composed with two section, ρ step and $V(\triangle x[k])$ step. ρ step is to find maximum sublevel set of $V(\triangle x[k])$ (since, $\{\triangle x[k]|V(\triangle x[k]) - \rho \geq 0\} \subset \{\triangle x[k]| - (dV(\triangle x[k]) + \epsilon \triangle x^T[k] \triangle$

$x[k]) \geq 0\}$, $\{\triangle x[k] | V(\triangle x[k]) - \rho \geq 0\}$ is BoA). $V(\triangle x[k])$ step is finding a new Lyapunov function at least good as previous one. After iterations, we can get estimated basin of attraction with Lyapunov function.

3.5 Feedback Control

To enlarge basin of attraction around the fixed point, we will use feedback controller to our system [58, 59]. Discrete linear quadratic regulator(DLQR) will be applied to get feedback gain of the feedback controlled system. Before applying feedback controller, we need to clarify the Poincaré return map of the system which starts from the end of posterior leg stance phase. Linearized Poincaré return map at the fixed point is

$$\begin{aligned} x^p[k+1] &= P(x^p[k], \alpha_{total}[k]) \\ \triangle x^p[k+1] &= A \triangle x^p[k] + B \triangle \alpha_{total}[k]. \end{aligned} \tag{3.23}$$

Let p is fixed point of state (x) and r is corresponding parameter variable set, then $\triangle x = x - p$, $\triangle \alpha = \alpha - r$, $A = \frac{\partial P}{\partial x}|_{x=p}$, and $B = \frac{\partial P}{\partial \alpha}|_{\alpha=r}$. Let K be feedback gain, then we can make input parameter set as $\triangle \alpha_{total}[k] = -K \triangle x^p[k]$, then the linearized Poincaré return map is

$$\triangle x^p[k+1] = (A - BK) \triangle x^p[k]. \tag{3.24}$$

Therefore, we can make eigenvalues of A-BK located in unit circle to make fixed point of the system locally asymptotically stable.

3.5.1 Discrete Linear Quadratic Regulator

As mentioned above, defining feedback gain K is important to make the feedback controlled system to have asymptotically stable behavior around fixed point. Since 3.21

is linear dynamic equation, convexity is ensured. So, $\triangle x^p[k]$ and $\triangle \alpha_{total}[k]$ are convex. Therefore, we can set our cost function (J) [61] to minimize as

$$min\ J = \frac{1}{2}\sum_{k=1}^{\infty}(z^T[k]Qz[k] + \beta^T[k]R\beta[k] + 2z^T[k]N\beta[k]), \tag{3.25}$$

where $\triangle x^p[k] = z[k]$ and $\triangle \alpha_{total}[k] = \beta[k]$. The optimal input minimizing the cost function(J) is given as $z[k] = -K\beta[k]$. By minimizing this cost function, we can choose feedback gain K which also minimizes $z[k]$ and $\beta[k]$. To make good performance of feedback controller to enlarge BoA around fixed point, we will set Q, R, and N matrix [60] used in cost function as

$$\begin{aligned}
Q &= diag(\frac{1}{max|z[k]_1|}, \frac{1}{max|z[k]_2|}, \frac{1}{max|z[k]_3|}, \frac{1}{max|z[k]_4|}, \frac{1}{max|z[k]_5|}, \frac{1}{max|z[k]_6|}),\\
R &= diag(\frac{1}{max|\beta[k]_1|}, \frac{1}{max|\beta[k]_2|}, \frac{1}{max|\beta[k]_3|}, \frac{1}{max|\beta[k]_4|}, \frac{1}{max|\beta[k]_5|}, \frac{1}{max|\beta[k]_6|}),\\
N &= 0,
\end{aligned} \tag{3.26}$$

where diag(a) is the $N \times N$ diagonal matrix whose entries are the N elements of the vector a. $z[k]_i$ is i-th component of z[k]. $\beta[k]_i$ is i-th component of $\beta[k]$.

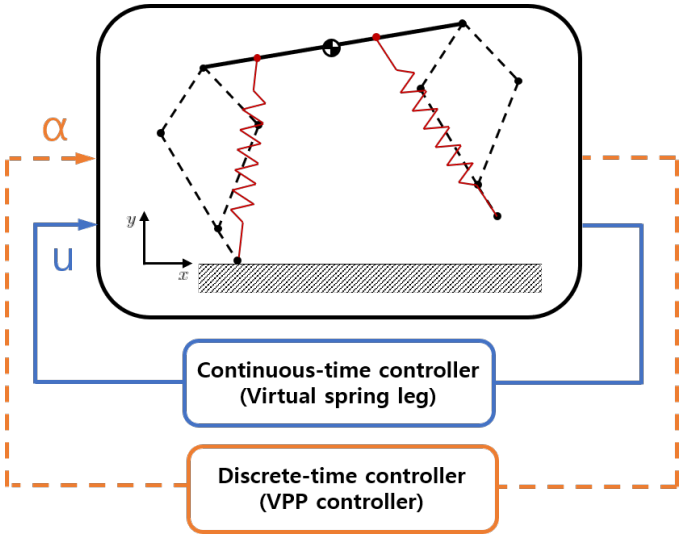

Figure 3.3: Feedback diagram structure for VPP controller. Continuous time signals are represented as continuous lines. Dashed time signals are represented as dash lines.

Using feedback controller and VPP control method, feedback diagram structure of the system can be described as Fig. 3.3.

Chapter 4

SIMULATION RESULTS

This chapter consists of three parts. The first part evaluates the stability properties of the proposed VPP controller via simulation. The system will experience unexpected ground height variations during the simulation. The stability of VPP controlled and passive bounding gait will be assessed by simulation results. The second part compares the simulation results of adjusted input parameter sets. The third part constructs a safe transition map between periodic orbits with different forward speeds.

4.1 Stability Analysis for VPP Controller

4.1.1 Passive Periodic Bounding Gait

A number of constraints are applied to the system to conduct bounding gait motion. List of constraints are

- Ground reaction force vector should be located in friction cone.
- Actuator torques cannot exceed the motor saturation limit.
- Model should move forward for each phase.
- Model should not experience double stance phase during bounding gait motion.
- Each phase should be conducted in order.

From Chapter 3, the Poincaré section is decided to be the end of posterior stance phase to eliminate non-repeating state variable "x" from state variables in the Poincaré section. Therefore, bounding gait motion in this simulation starts at right before lift-off from the ground during posterior leg stance phase. Periodic orbit and corresponding fixed point of the passive bounding gait system is computed. The fixed point consists

of the initial state (x^*) and corresponding input parameter value set(α^*). The initial state (x^*) and corresponding input parameter value set(α^*) for the passive bounding gait system are

$$\begin{aligned}(x^p)^* &= [q^{p*}, \dot{q}^{p*}]^\top = [3.1784, 0.1305, 0.0288, -16.6392, 12.4912, -6.7321]^\top, \\ (\alpha)^* &= [k^p, k^a, l_v^p, \theta_{td}^p, l_v^a, \theta_{td}^a]^\top = [2300, 2300, 0.2, 1.8294, 0.2, 1.5632]^\top,\end{aligned} \tag{4.1}$$

where notations are described in Table 2.3. By linearizing the Poincaré return map at the fixed point, we can evaluate the stability of the system around the fixed point. This evaluation is conducted by comparing eigenvalues of fixed point whether they are located within the unit circle. Corresponding eigenvalues of the fixed point are

$$\begin{aligned}e_{passive} &= [-0.92571 + 0.13698i, -0.92571 - 0.13698i, 0.9999999]^\top, \\ max(|e_{passive}|) &= 0.9999999.\end{aligned} \tag{4.2}$$

Since all eigenvalues are located in the unit circle, the fixed point is asymptotically stable. To evaluate the periodic motion of the system when the state is at a fixed point, 3 steps of passive bounding gait are conducted. Passive bounding gait motion shows a peak forward speed of 1.15m/s and moves 0.4263 m forward.

Fig. 4.1 shows state variables with respect to time. The black line is the trajectory of state variable during bounding gait, blue dash line is the initial value of state variable, and the red dot is the return value of the Poincaré return map when one cycle of bounding gait is ended. From Fig. 4.1, we can observe that the state does repeating motion and has the same value when one cycle of bounding gait is ended. Corresponding actuator input, ground reaction force, and virtual leg length change are described in Fig. 4.2.

In Fig. 4.2e, the red line is for the virtual spring leg for the anterior leg, and the blue dash line is for the posterior leg. In Fig. 4.2f, the red line corresponds to vertical ground reaction force applied on point foot, and the blue dash line corresponds to horizontal ground reaction force. To evaluate constraints related to actuator torques

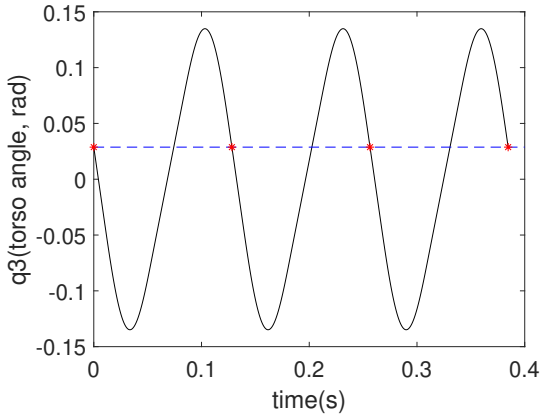

(a) Torso angle

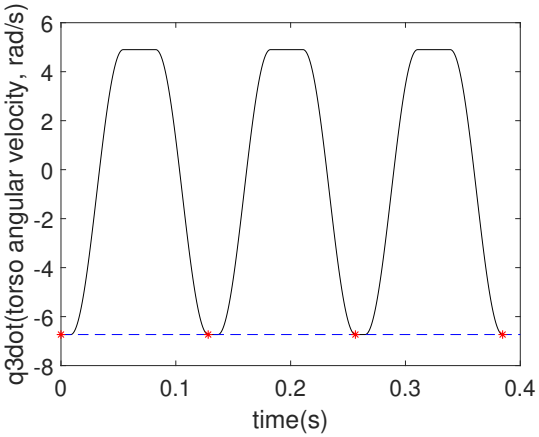

(b) Torso angular velocity

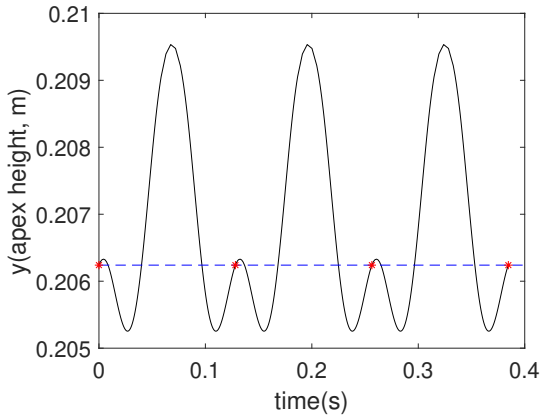

(c) Torso vertical location

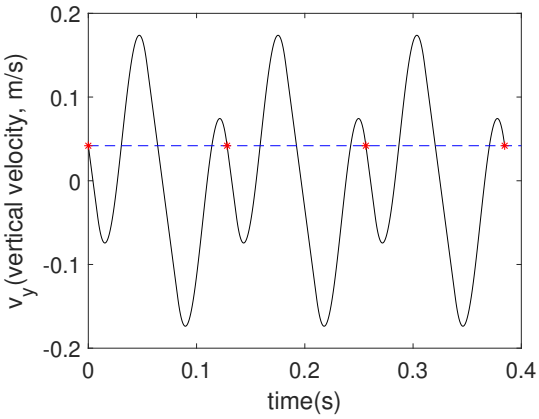

(d) Torso vertical velocity

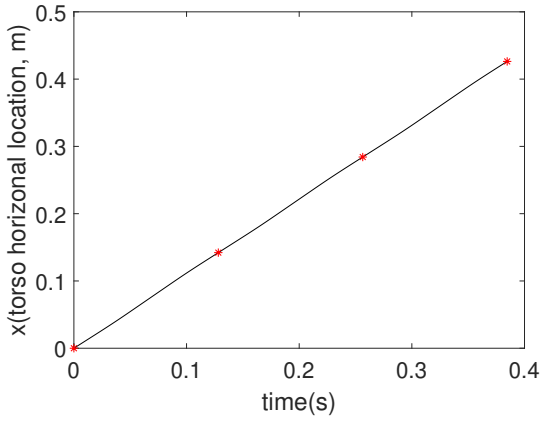

(e) Torso horizontal location

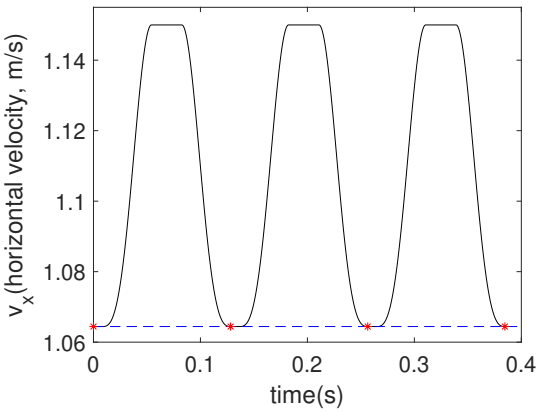

(f) Torso horizontal velocity

Figure 4.1: State variables during three steps of passive bounding gait

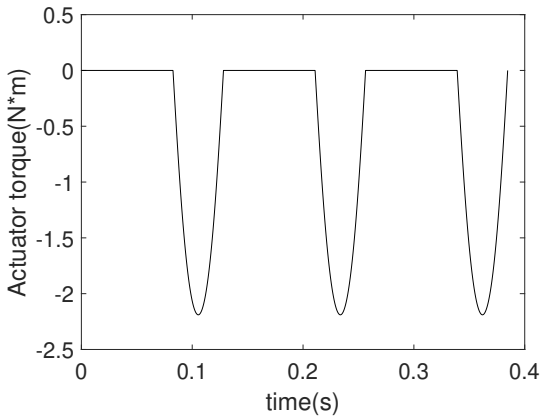

(a) 1_{st} posterior actuator

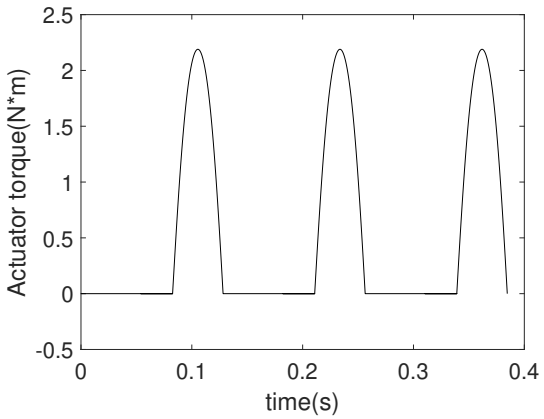

(b) 2_{nd} posterior actuator

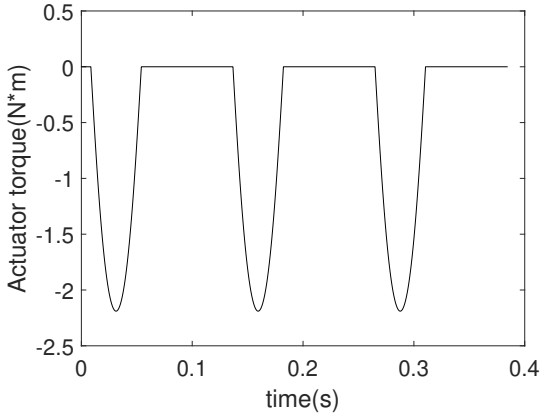

(c) 1_{st} anterior actuator

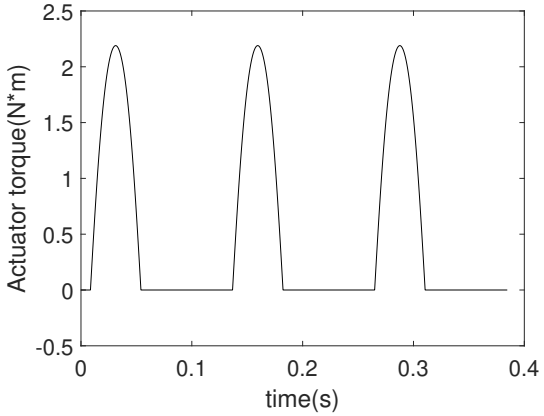

(d) 2_{nd} anterior actuator

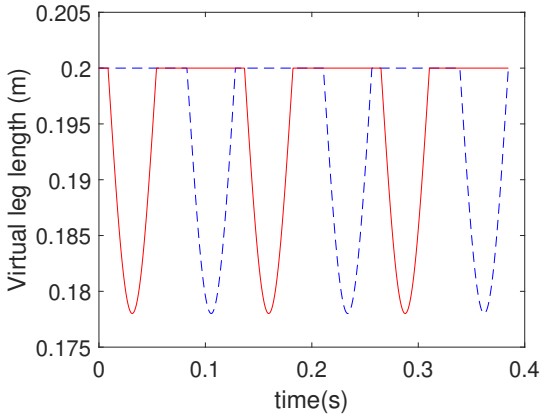

(e) Virtual spring leg

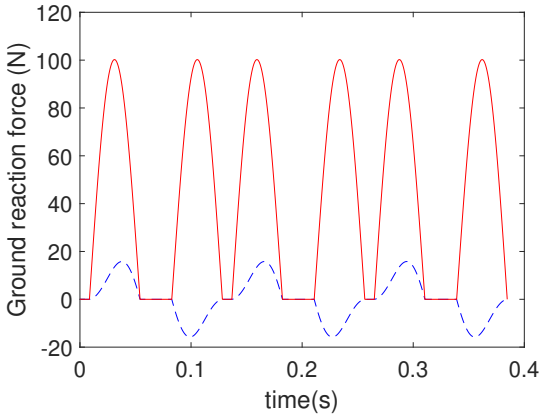

(f) Ground reaction force

Figure 4.2: Actuator input, virtual leg, and ground reaction force in three steps of passive bounding gait

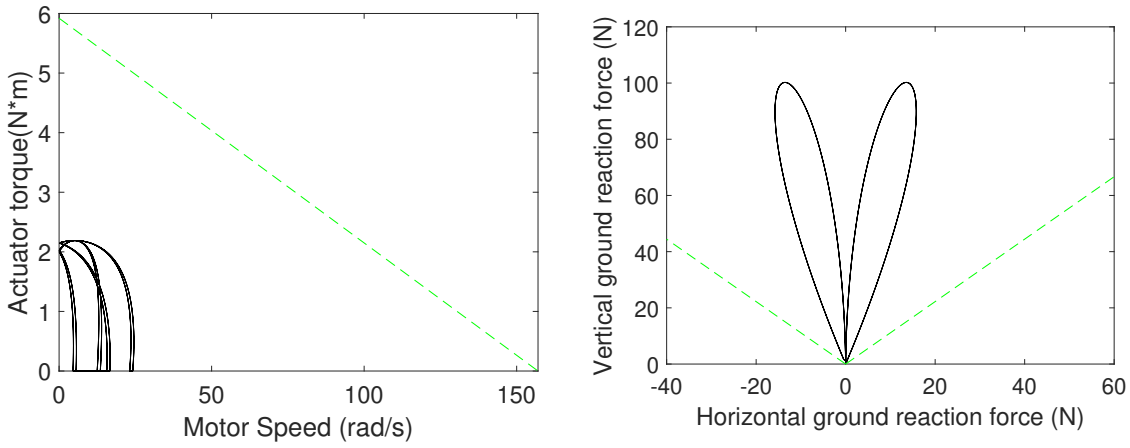

(a) Actuator torque and motor limit

(b) Ground reaction force

Figure 4.3: Motor torque with motor saturation limit and ground reaction force with friction cone

and ground reaction forces, actuator torque and ground reaction force graphs will be redrawn in Fig. 4.3.

In Fig. 4.3a green dash line is motor limit and saturation occurs when motor input reaches this limit. In Fig. 4.3b, the green dash line is the largest allowable friction ration that the model can have. Required friction ratio is computed by $\frac{GRF_h}{GRF_v}$ (GRF_h : horizontal ground reaction force, GRF_v : vertical ground reaction force). Fig. 4.3 shows actuator torque, and ground reaction force while conducting three steps bounding gait described in Fig. 4.1. In Fig. 4.3, the largest value of torque is 2.1896 Nm and the fastest motor speed is 24.5164 rad/s. Therefore, all actuator torques are located within the given motor limit. For ground reaction force (GRF), the largest required friction ratio is 0.2642 and this value is smaller than 0.9 which is the largest friction ratio that the system can have. Fig. 4.1, 4.2, and 4.3 indicate that the bounding gait motion of the system shows repeating motion and satisfies constraints. These results will be compared with the VPP controlled bounding gait motion.

4.1.2 VPP Controlled Bounding Gait

To apply the VPP controller to the passive bounding gait system, two more input parameters d_p, and d_a are needed. d_p, and d_a indicate distance between the virtual pivot point and the hip joint of the model. Initial state (x^*_{vpp}) and corresponding input parameter value set(α^*_{vpp}) of VPP controlled bounding gait are

$$\begin{aligned} x^{p*}_{vpp} &= [q^{p*}, \dot{q}^{p*}]^\top = [3.1784, 0.1305, 0.0288, -16.6392, 12.4912, -6.7321]^\top, \\ (\alpha)^*_{vpp} &= [k^p, k^a, d_p, d_a, l^p_v, \theta^p_{td}, l^a_v, \theta^a_{td}]^\top = [2300, 2300, 0, 0, 0.2, 1.8294, 0.2, 1.5632]^\top. \end{aligned} \tag{4.3}$$

4.1.3 Unexpected Ground Height Variation Test

In this section, we will estimate BoA around fixed points of the passive bounding gait and VPP controlled bounding gait system and compare two results. Before estimating the BoA, the feedback controller will be applied to enlarge the BoA for each case. Feedback gain is computed by discrete linear quadratic regulator (DLQR). Q, R, and N matrices for tuning DLQR are decided by the difference between maximum and minimum state and input values. Q, R, and N matrices are

$$\begin{aligned} Q &= diag(4, 4, 4, 0.01, 0.01, 0.01), \\ R &= diag(\frac{1}{4000^2}, \frac{1}{4000^2}, \frac{1}{0.2^2}, \frac{1}{0.2^2}, \frac{1}{0.22^2}, \frac{1}{2^2}, \frac{1}{0.22^2}, \frac{1}{2^2}, \frac{1}{2^2}, \frac{1}{2^2}), \\ N &= 0, \end{aligned} \tag{4.4}$$

where diag(a) is the $N \times N$ diagonal matrix whose entries are the N elements of the vector a. After applying the feedback controller, eigenvalues of linearized Poincaré return map for passive bounding gait are

$$\begin{aligned} e_{passive} = [0.75337, -0.57246, 0.05135, -0.00127, -6.07069 * 10^{-9}, 3.72842 * 10^{-9}]^\top, \\ max(|e_{passive}|) = 0.75337. \end{aligned} \tag{4.5}$$

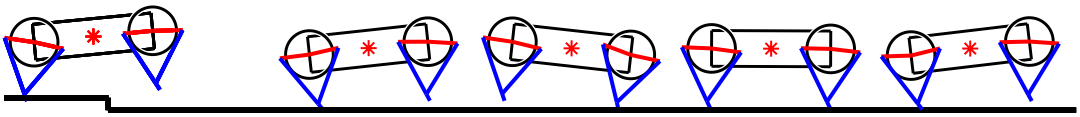

Figure 4.4: Snapshots of the model running down a step of 4.1 cm ground height variation (20% of the nominal leg length).

Since all eigenvalues are located in the unit circle, the fixed point of passive bounding gait is still asymptotically stable. The maximum absolute eigenvalue is decreased from the case when the feedback controller is not applied. This decreased eigenvalue indicates faster converging motion around a fixed point. Eigenvalues of linearized Poincaré return map for VPP controlled bounding gait are

$$e_{vpp} = [-0.43625, 0.48602, 0.01350, -0.01092, -1.00489 * 10^{-8}, 2.59274 * 10^{-9}]^{\top},$$
$$max(|e_{vpp}|) = 0.48602. \tag{4.6}$$

The fixed point of VPP controlled bounding gait is also asymptotically stable since all eigenvalues are also located within the unit circle.

To compare the stability of passive and VPP controlled bounding gait systems, the model will experience unexpected ground height variation. Variation in the ground height is equal to 20% of the virtual leg length. Fig. 4.4 indicates snapshots of the system's motion on converging to the nominal bounding motion which corresponds to a periodic orbit of the system. In Fig. 4.4, the first 2 steps are experiencing different ground levels of the posterior and anterior leg, and the remaining 18 steps are on flat ground with lower ground height.

In Fig. 4.5 and 4.6, the black line is state change during bounding gait, blue dash line is the fixed point value of the state, and the red dot is the return value of the Poincaré return map when one step of bounding gait is ended. In Fig. 4.5 indicates that the passive bounding gait system is not converging to its nominal bounding gait motion. Fig. 4.6 indicates VPP controlled bounding gait ability to make the system converge to its nominal bounding gait motion.

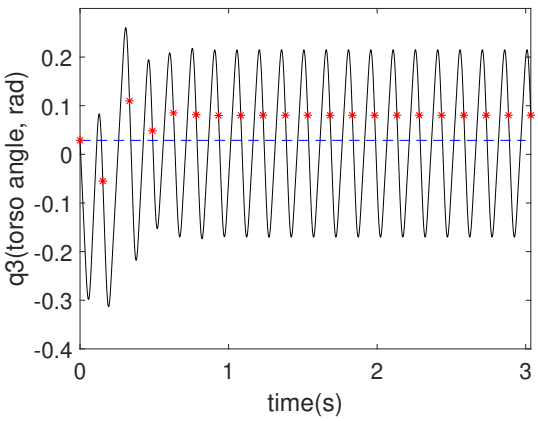

(a) Torso angle

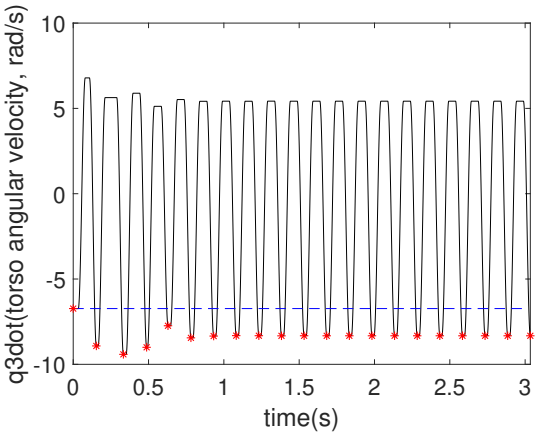

(b) Torso angular velocity

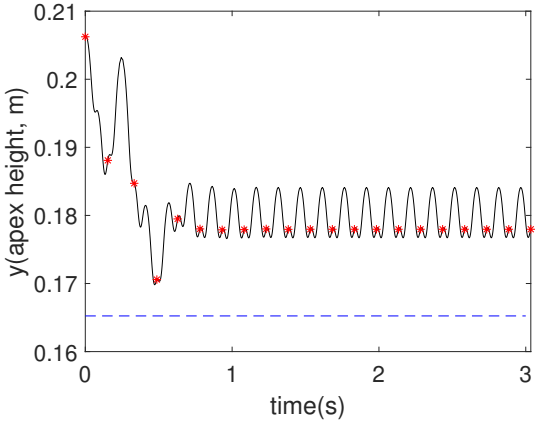

(c) Torso vertical location

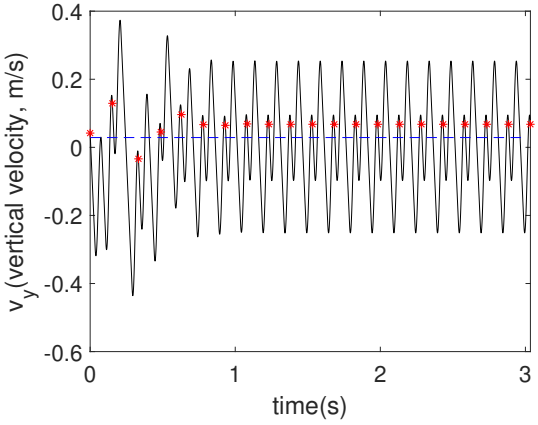

(d) Torso vertical velocity

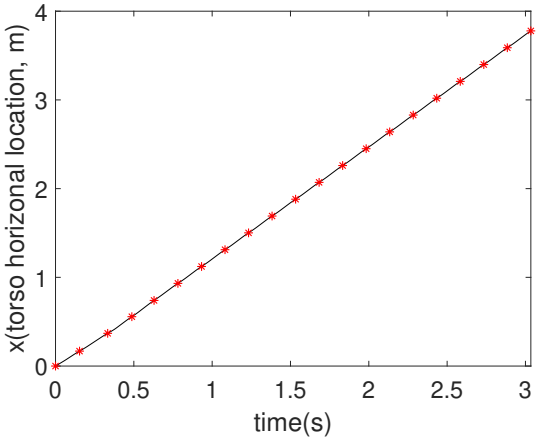

(e) Torso horizontal location

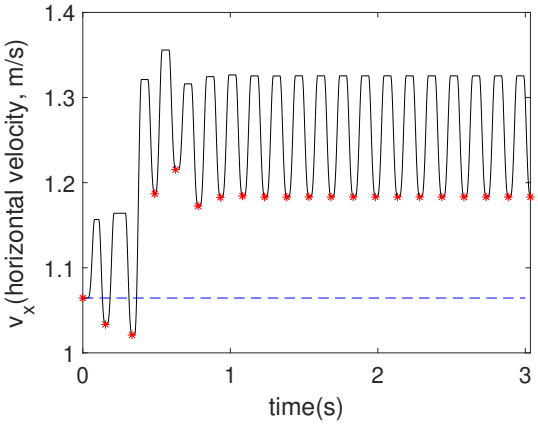

(f) Torso horizontal velocity

Figure 4.5: State variables of passive bounding gait system during unexpected ground level variation test

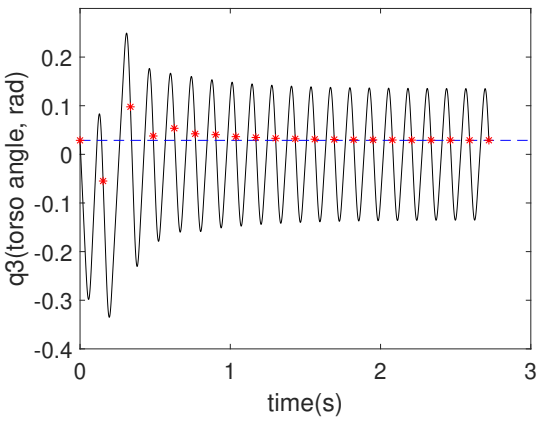

(a) Torso angle

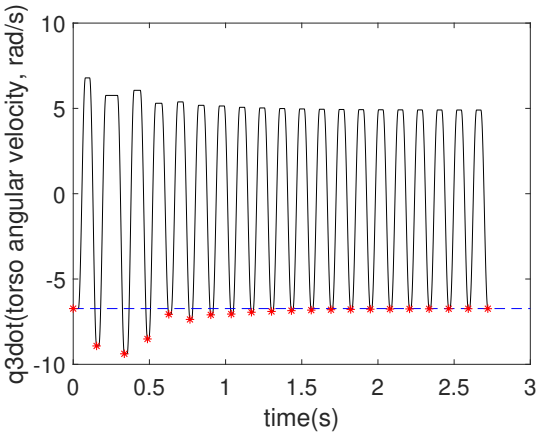

(b) Torso angular velocity

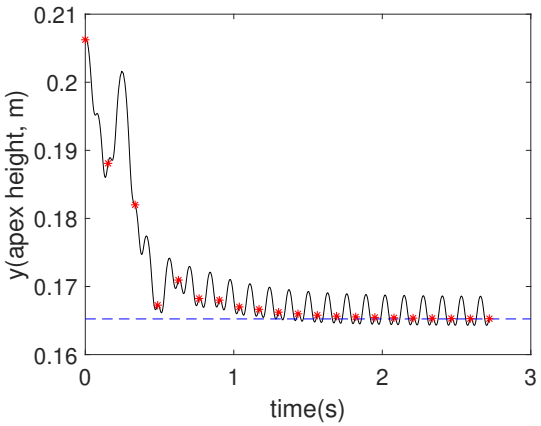

(c) Torso vertical location

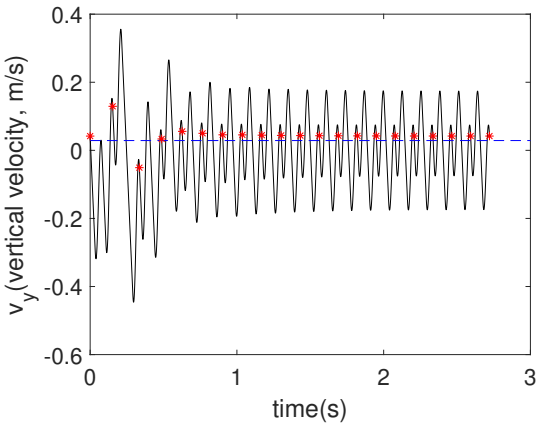

(d) Torso vertical velocity

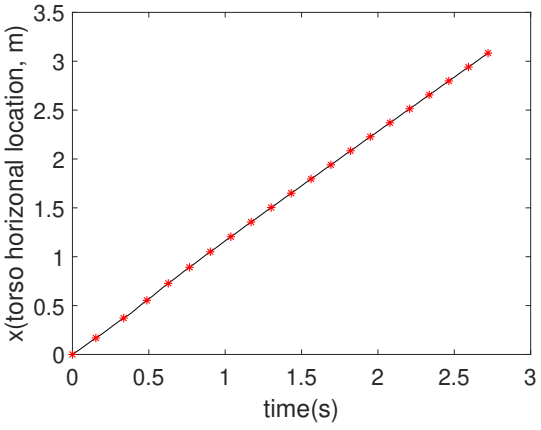

(e) Torso horizontal location

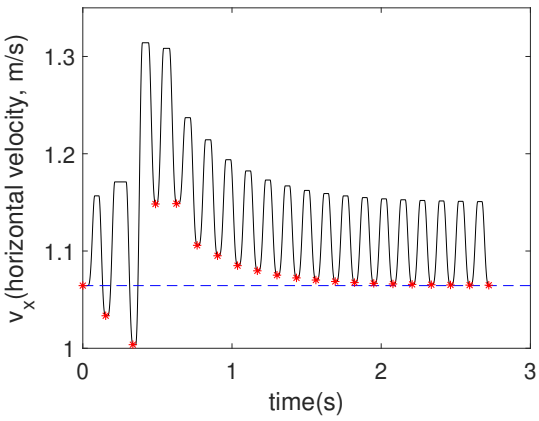

(f) Torso horizontal velocity

Figure 4.6: State variables of VPP controlled bounding gait system during unexpected ground level variation test

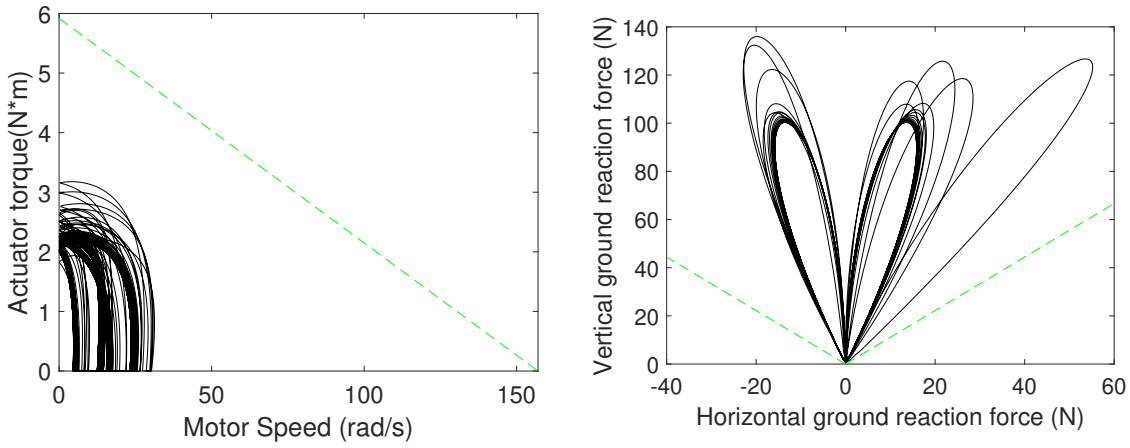

(a) Actuator torque and motor limit

(b) Ground reaction force

Figure 4.7: Motor torque and Ground reaction force of VPP controlled bounding gait motion during unexpected ground level variation test

In Fig. 4.7, the system is satisfying constraints during the ground level perturbation test. All actuator input and ground reaction vector are located within its limit (green dash line).

In Fig. 4.8, the blue dash line is a fixed point energy level of lower ground level and the red dot is initial total energy level. Fig. 4.8 indicates total energy level changes of the passive bounding gait and VPP controlled bounding gait system during the ground level perturbation test. The passive bounding gait system cannot converge to its nominal energy level (Fig. 4.8a). VPP controlled bounding gait system is able to establish convergence to its nominal energy level.

4.1.4 Adjusted Input Parameter Set

Inspired from symmetry characteristics of passively generated bounding gait leg motions on quadruped robots, the number of input parameter variables will be adjusted. Unexpected ground level change test is conducted to compare the results of applying symmetric relation between the touchdown and lift-off angles of legs. The

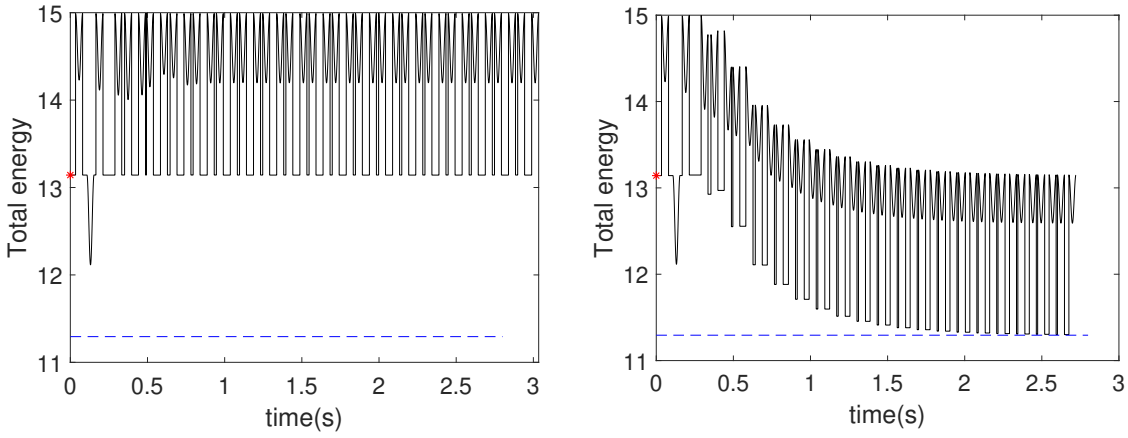

(a) Passive bounding gait system (b) VPP controlled bounding gait system

Figure 4.8: Total energy level during ground level perturbation test

symmetric relationship between touchdown and lift-off angle is

$$\begin{cases} \theta^p_{td} = -\theta^a_{lf} + \pi \\ \theta^a_{td} = -\theta^p_{lf} + \pi \end{cases}, \tag{4.7}$$

where "td" indicates touchdown and "lf" indicates lift-off. In addition, virtual leg length should be the same to make symmetric relationship. Input parameter set candidates are

$$\begin{aligned} \alpha_1 &= [k^p, k^a, d^p, d^a, l^p, \theta^p_{td}, l^a, \theta^a_{td}, p^p, p^a], \\ \alpha_2 &= [k^p, k^a, d^p, d^a, l^p, \theta^p_{td}, l^a, \theta^a_{td}], \\ \alpha_3 &= [k^p, k^a, d^p, d^a, l^p, \theta^p_{td}], \\ \alpha_4 &= [k^p, k^a, d^p, d^a], \end{aligned} \tag{4.8}$$

where p^p, and p^a are the spring force proportional ratio for the posterior and anterior leg. By using p^p, and p^a, we can directly control the virtual spring leg force. The input parameter set α_1 is for the system with additional leg thrust to control its total energy level, α_2 is the input parameter set we are using for VPP controller, α_3 is a reduced input parameter set by considering symmetric motion of animal, and α_4 is

for the case when virtual pivot point and virtual spring leg concepts are considered and symmetric motion of animal is ignored. Four cases of input set are compared by unexpected ground level perturbation test and the results are

Table 4.1: Maximum step down perturbation for input parameter set candidates

α	1_{st} case input(α_1)	2_{nd} case input(α_2)	3_{rd} case input(α_3)	4_{th} case input(α_4)
δ	4.1 cm	4.1 cm	4.1 cm	0 cm

The parameter δ is maximum ground height perturbation that the system can converge to its nominal bounding gait motion. From Table 4.1, 3_{rd} case input (α_3) is the most optimal input set for VPP controller considering computational complexity and its performance. In the case of α_4, the system loses its ability for establishing convergence to its nominal bounding gait motion. This result indicates that the symmetric motion of animals directly affects the system's ability to make the system converge to its nominal motion. The result from the 1_{st} case indicates that an additional leg thrust controller has a small effect in enlarging BoA of the system.

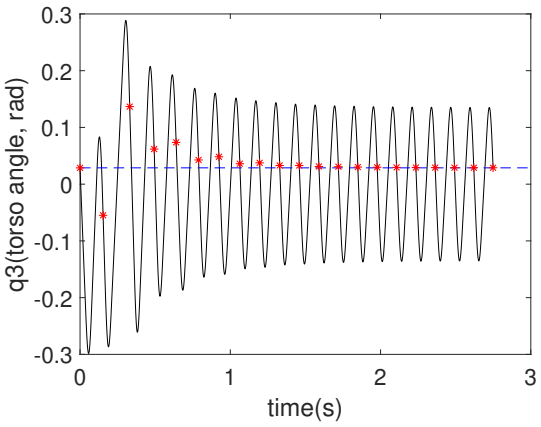

(a) Torso angle

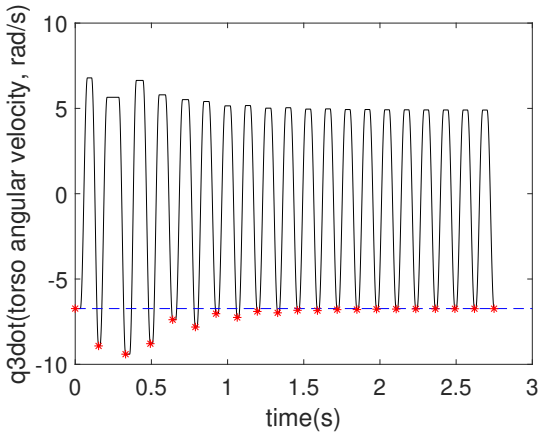

(b) Torso angular velocity

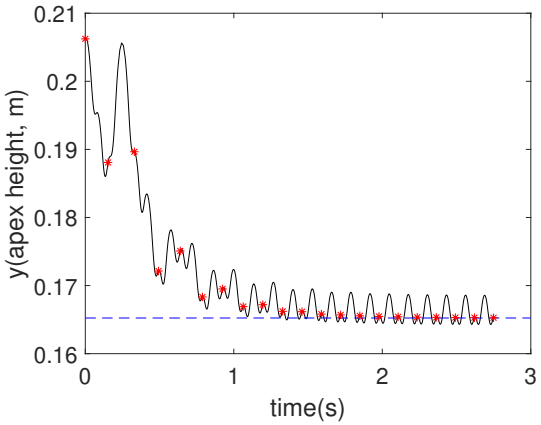

(c) Torso vertical location

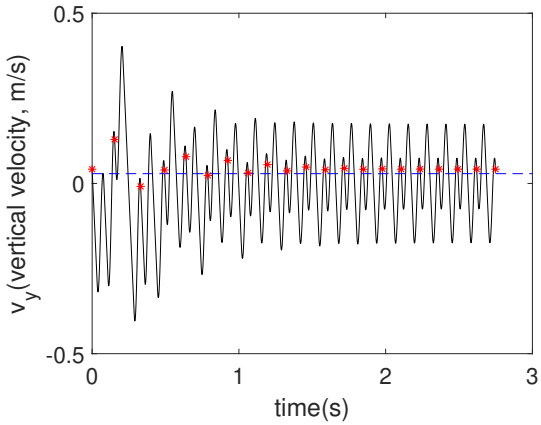

(d) Torso vertical velocity

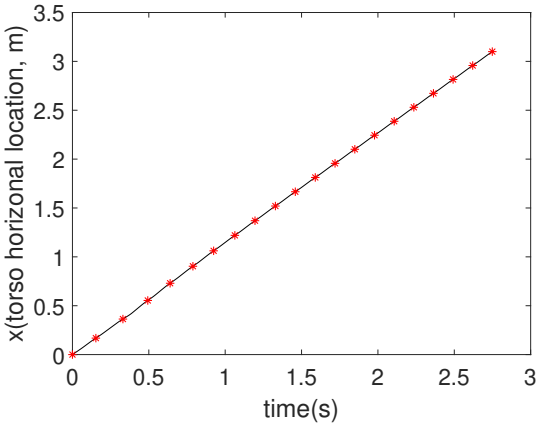

(e) Torso horizontal location

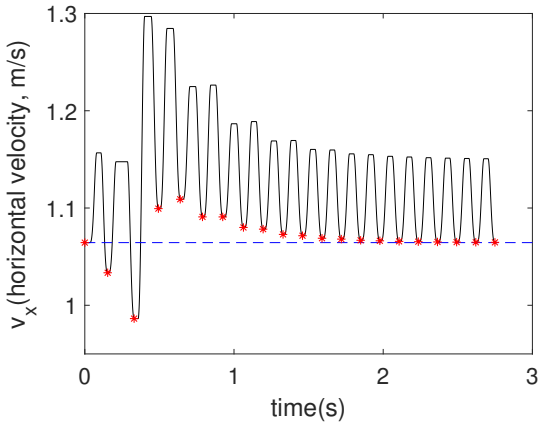

(f) Torso horizontal velocity

Figure 4.9: Step down perturbation test for reduced input set (α_3) of VPP controlled bounding gait

Comparing Fig. 4.6 and Fig. 4.9 which are results from unexpected ground height perturbation test for α_2 and α_3 cases, both systems maintain its ability to make the system converge to its nominal bounding gait motion.

4.2 Speed Transition Simulation

In this section, we will construct safe transition map between periodic orbits with different forward speeds.

4.2.1 Fixed Points with Different Speeds

Eight different fixed points with different forward speeds are evaluated and initial states and corresponding input parameter sets are

v_x (m/s)	$x^p = [q_1^p, q_2^p, q_3, \dot{q}_1^p, \dot{q}_2^p, \dot{q}_3]$					
0.8	3.1908	0.1429	0.2523	-32.2444	14.4301	-10.5010
1.15	3.1784	0.1305	0.0288	-16.6392	12.4912	-6.7321
1.2	3.1862	0.1383	0.1226	-25.5793	14.9216	-9.4308
1.4	3.2096	0.1617	0.0409	-20.5755	14.9803	-8.1216
1.6	3.2681	0.1922	0.0533	-21.8132	16.6627	-8.4822
1.75	3.3111	0.2131	0.0625	-22.7565	17.9550	-8.7381
2.05	3.3476	0.2795	0.0834	-24.7024	19.9655	-9.3943
2.25	3.3851	0.3170	0.0958	-25.8193	21.4268	-9.6955

Table 4.2: Initial state in fixed points with different forward speeds

v_x (m/s)	$\alpha = [k^p, k^a, d^p, d^a, l^p, \theta^p_{td}]$					
0.8	2800	2800	0	0	0.2	1.9168
1.15	2300	2300	0	0	0.2	1.8294
1.2	2300	2300	0	0	0.2	1.9081
1.4	1800	1800	0	0	0.2	1.8963
1.6	1800.0079	1800.0078	0	0	0.1986	1.9115
1.75	1800.0120	1800.0116	0	0	0.1975	1.9240
2.05	1800.0250	1800.0246	0	0	0.1990	1.9521
2.25	1800.0324	1800.0319	0	0	0.1990	1.9680

Table 4.3: Input parameter variable set with different forward speeds

Each fixed point's local stability is evaluated by computing eigenvalues of linearized Poincaré return map at each fixed point. Corresponding maximum eigenvalues for fixed points with different forward speeds are

$$\begin{aligned} max(|e_{v_x=0.8}|) &= 0.6027, \\ max(|e_{v_x=1.2}|) &= 0.5693, \\ max(|e_{v_x=1.4}|) &= 0.5628, \\ max(|e_{v_x=1.6}|) &= 0.5536, \\ max(|e_{v_x=1.75}|) &= 0.5474, \\ max(|e_{v_x=2.05}|) &= 0.5494, \\ max(|e_{v_x=2.25}|) &= 0.5494. \end{aligned} \tag{4.9}$$

Since all eigenvalues for each case are located in the unit circle, all the fixed points are asymptotically stable.

4.2.2 Basin of Attraction Estimation

This section estimates basin of attraction (BoA) of fixed points (4.2 and 4.3). Using the method described in Chapter 3, BoA is estimated (Appendix B). To conduct

a safe transition between periodic orbits with different forward speeds, each fixed point should be located in other fixed point's BoA.

Table 4.4: Fixed points and estimated BoA relations

from (m/s) \ to (m/s)	0.8	1.15	1.2	1.4	1.6	1.75	2.05	2.25
0.8	-	O	O	O	X	X	X	X
1.15	O	-	O	O	O	O	O	X
1.2	O	O	-	O	O	O	O	O
1.4	O	O	O	-	O	O	O	O
1.6	X	O	O	O	-	O	O	O
1.75	X	O	O	O	O	-	O	O
2.05	X	O	O	O	O	O	-	O
2.25	X	O	O	O	O	O	O	-

In Table 4.4, "O" indicates that fixed point is located in estimated BoA of fixed point with objective speed and "X" means that fixed point is not located in estimated BoA of fixed point with objective speed. Since the estimated BoA is not actual BoA, we will conduct actual simulation for verifying these relations (Table 4.4) especially for the transition with the largest forward speed difference.

4.2.3 Speed Transition Result

This section simulates forward speed transition of the system. Connected fixed points, which indicates one fixed point is located in other fixed point's BoA, with the largest difference in speed ($2.25m/s \rightarrow 1.15m/s$) will be simulated for forward speed transition. Speed transition result are described in Fig. 4.10.

In Fig. 4.10, speed transition between $v_x = 2.25m/s$ and $v_x = 1.15m/s$ is successfully conducted. In Fig. 4.11, all actuator torque and ground reaction forces satisfy constraints. Fig. 4.11a shows that motor torque approximate its limit and this

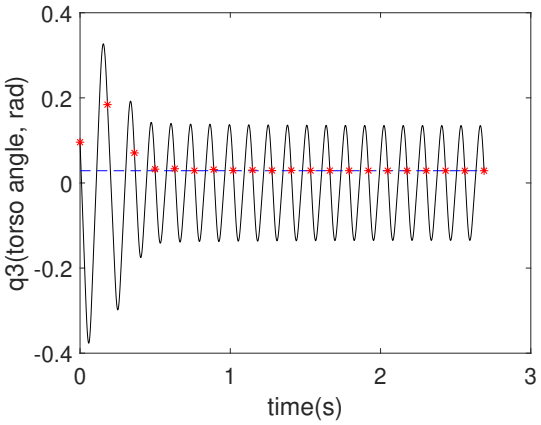

(a) Torso angle

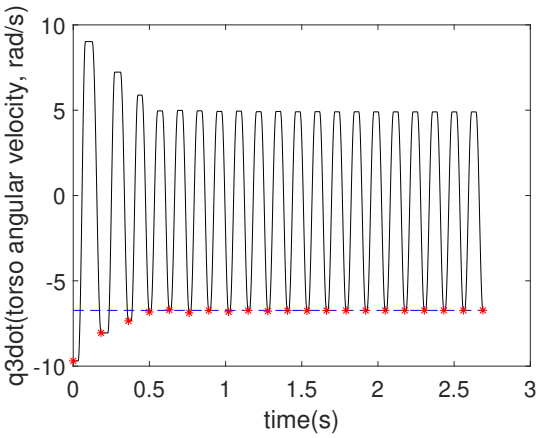

(b) Torso angular velocity

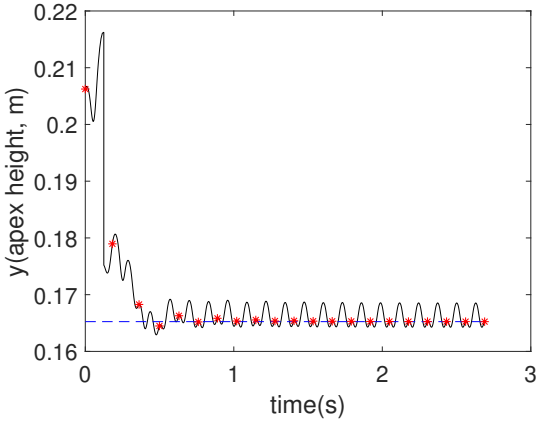

(c) Torso vertical location

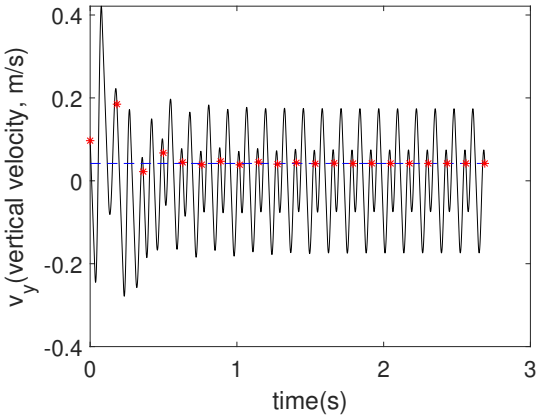

(d) Torso vertical velocity

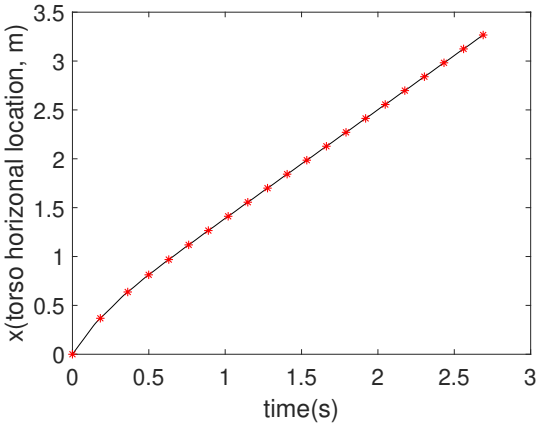

(e) Torso horizontal location

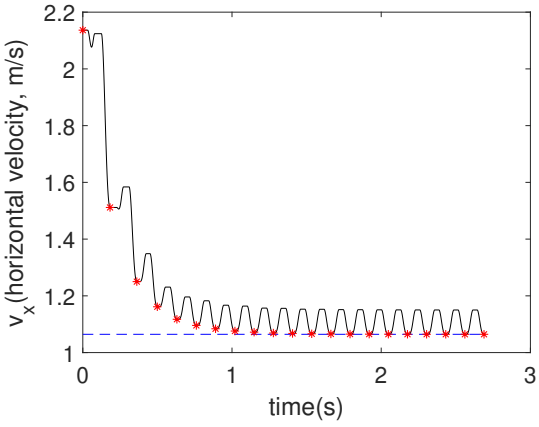

(f) Torso horizontal velocity

Figure 4.10: Forward speed transition from $v_x = 2.25m/s$ to $v_x = 1.15m/s$

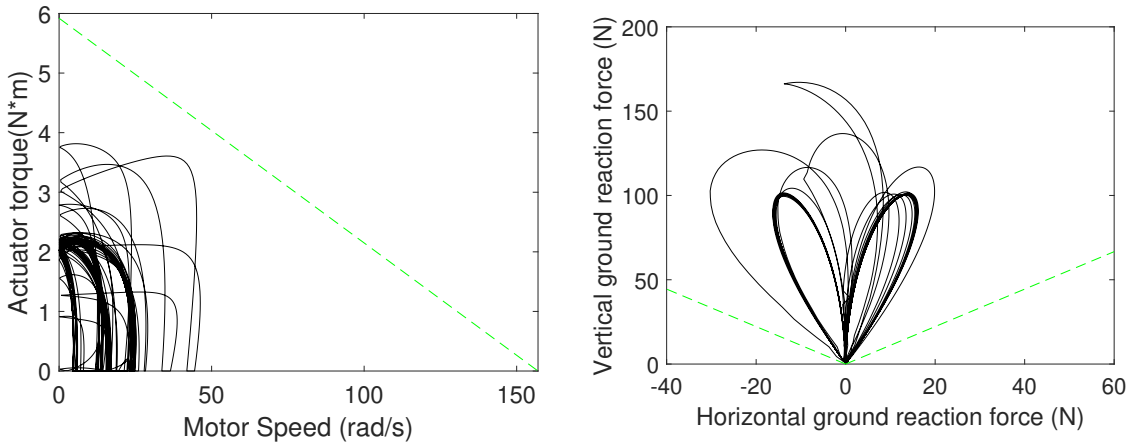

(a) Actuator torque and motor limit

(b) Ground reaction force

Figure 4.11: Motor torque and Ground reaction force

is the main reason to fail transition among larger difference in forward speeds such as $v_x = 2.25m/s$ to $v_x = 0.8m/s$.

Chapter 5

CONCLUSIONS AND FUTURE WORK

This chapter provides a brief summary of the results presented in this thesis and perspectives on future work on the virtual pivot point (VPP) control method used for the bounding gait of quadrupedal robots.

5.1 Conclusions

A lot of research has been focused on quadrupedal bounding gait. However, the majority of research control bounding gait motion by the continuous-time controller and evaluate stability properties by simulating on flat ground. In this thesis, we proposed a novel discrete-time control method for quadruped bounding gait. By introducing a discrete-time control method and computing the passive periodic orbit of the system, we could reduce the computational demands of the system [19] compared to the previous continuous-time control methods. The periodic motion of the passive bounding gait system was well shown in Fig. 4.1. The stability of the system was evaluated by computing eigenvalues of the linearized Poincaré return map and simulating unexpected ground height variation simulation. The basin of attraction, which is directly related to the system's convergence to nominal bounding gait motion, was enlarged by the VPP controller. From Fig. 4.6, the system was able to converge back to its nominal bounding gait motion under the influence of ground level perturbation only when the VPP controller was applied.

The computational complexity of the VPP controller was reduced by decreasing the number of input parameter variables. Since feedback gain of the system was computed by discrete linear quadratic regulator, the size of matrices directly influences

computation complexity to compute feedback gain. Inspired from symmetry characteristics of passively generated bounding gait leg motions, we could reduce the number of input parameter variables from eight to six and the size of R matrix (3.26) was reduced from 8×8 to 6×6.

Safe transition map between periodic orbits with different forward speeds was constructed and simulated. Basin of attraction for each periodic orbit with different speeds was estimated by using a sum of square method. With the use of estimated basins of attraction, we could map the relation of each fixed point whether they are in other fixed points' basin of attraction. This map was verified by the speed transition simulation. Two fixed points, which are connected but have the largest different forward speed, were used for speed transition simulation and results in successful speed transition from 2.25 m/s to 1.15 m/s.

5.2 Perspectives on Future Work

In this thesis, we suggested a discrete control method for quadrupedal bounding gait and verified its ability to converge nominal bounding gait motion. As shown in Chapter 4, constraints on actuator torques and friction ratio play a key role in making the system to have a periodic motion for bounding gait. Therefore, the most natural direction for research in quadrupedal robot bounding gait is improving the VPP controller in the aspect of constraints or input parameter set.

The VPP controller described in this thesis used a parameter set as input. This parameter set will be converted to a function of feedback gain and state when the system is at the end of the posterior stance phase. Since the input parameter set includes touchdown angles, stiffness of virtual legs, virtual pivot point locations, and virtual leg lengths, nearly half of the input parameters are not used at the end of posterior stance phase. Therefore, when the anterior leg stance phase starts, the system is using past time feedback input parameters. Since we are using discrete Poincaré return map for evaluating the stability properties of a periodic orbit, applying real-time feedback is not possible. Therefore, more studies toward a system with multiple

Poincaré sections are needed. When it is possible to provide feedback at the end of each phase, we could have feedback with more recent state information.

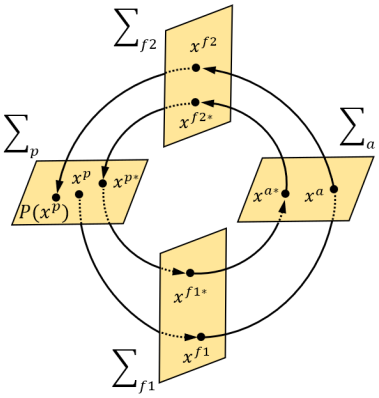

Figure 5.1: Poincaré return map with multiple Poincaré section

In Fig. 5.1, $\sum_{pl}$ and $\sum_{al}$ are Poincaré sections at the end of posterior and anterior leg stance phases, respectively. $\sum_{at}$ and $\sum_{pt}$ are Poincaré sections at the end of flight phases. x^{p}, x^{a}, x^{f1}, and x^{f2} are states for each Poincaré sections and $P(\cdot)$ is the full Poincaré return map of the system. x^{p*}, x^{a*}, x^{f1*}, and x^{f2*} are fixed point states for each Poincaré section.

Our perturbed simulation in Chapter 4 was conducted for unexpected 4.1 cm down stepping simulation. When perturbation was bigger than 4.1 cm, the system lost its ability to establish convergence to nominal bounding gait. The main reasons for this failure were constraints of motor saturation and friction ratio. When the anterior leg was touching the lower ground and the virtual spring leg was fully compressed, the required leg thrust exceeded the actuator limit. It is possible to reduce the required actuator torque by using feedback input parameters such as virtual leg length and stiffness. However, as mentioned above, the system is not capable of getting feedback input

in real-time and does not know whether there will be perturbation. Therefore, prediction of perturbed cases cannot be used in this situation and an additional controller to deal with perturbation is needed. By reducing the amount of torque required during perturbed bounding gait, the system will be able to withstand more perturbation.

In summary, there still exists a long path of research to make quadrupedal robots useful in our daily lives. The first objective is to make the quadrupedal robots move in a more robust way in diverse terrain types. The next objective is then making quadrupedal robots useful in humans' lives. Besides load carrying or delivering by quadrupedal robots, replacing people who work in dangerous environments is also a meaningful way to use quadrupedal robots.

BIBLIOGRAPHY

[1] G.A. Pratt "Legged robots at MIT: what's new since Raibert?" *IEEE Robotics & Automation Magazine*, 2000.

[2] Marc H. Raibert "Legged Robots that Balance." *MIT Press*, 1986.

[3] Marc H. Raibert "Running on Four Legs As Though They Were One" *IEEE Journal of Robotics and Automation*, 1986.

[4] Marc H. Raibert *Autonomous Robot Vehicles*. Springer, 1986.

[5] Andrew A. Biewener and C. Richard Taylor "Bone strain: a determinant of gait and speed?" *Journal of Experimental Biology*, 1986.

[6] Peter Feldmann "Homotopy Method for Finding the Steady States of Oscillators" *IEEE Transactions on Computer-Aided Design of Integrated Circuits and Systems*, 2014.

[7] K. Goldberg and Marc H. Raibert "Conditions for Symmetric Running in Single- and Double-Support" *IEEE International Conference on Robotics and Automation*, 1987.

[8] H.-M. Maus and S.W. Lipfert "Upright human gait did not provide a major mechanical challenge for our ancestors" *Nature Communications*, 2010.

[9] DV Lee and AA Biewener "BigDog-Inspired Studies in the Locomotion of Goats and Dogs" *Integrative and Comparative Biology*, 2011.

[10] M. Raibert, K. Blankespoor, G. Nelson, R. Playter, and the BigDog Team "BigDog, the rough-terrain quadruped robot" *The International Federation of Automatic Control*, 2008.

[11] J. Hamill, B. T. Bates, and K. M. Knutzen "Ground Reaction Force Symmetry during Walking and Running" *Research Quarterly for Exercise and Sport*, 2013.

[12] S. Talebi and I. Poulakakis "Quadruped Robot Running With a Bounding Gait" *Experimental Robotics VII*, 2002.

[13] Donald F. Hoyt and C. Richard Taylor "Gait and the energetics of locomotion in horses." *Nature 292.5820*, 1981.

[14] Tad McGeer "Passive dynamic walking" *The International Journal of Robotics Research*, 1990.

[15] Honda Corporation. Asimo's homepage. http://world.honda.com/asimo/. Technical report, 2013.

[16] Masato Hirose and Kenichi Ogawa "Honda humanoid robots development" *Philosophical Transactions of the Royal Society A: Mathematical, Physical and Engineering Sciences*, 2006.

[17] C. Chevallereau, G. Abba, Y. Aoustin, F. Plestan, E. R. Westervelt, Carlos Canudas-de Wit, and J.W. Grizzle "Rabbit: a testbed for advanced control theory" *IEEE Control Systems Magazine, 23(5):57–79*, 2003.

[18] Jessy W. Grizzle, Jonathan Hurst, Benjamin Morris, Hae-Won Park, and Koushil Sreenath "MABEL, a new robotic bipedal walker and runner" *In American Control Conference*, 2009.

[19] Kunlin Wei, Tjeerd MH Dijkstra, and Dagmar Sternad "Passive stability and active control in a rhythmic task." *Journal of Neurophysiology*, 2007.

[20] Tad McGeer "Passive dynamic walking." *I. J. Robotic Res.*, 1990.

[21] R. Bloss "Robot walks on all four legs and carries a heavy load" *Industrial Robot, Vol. 39*, 2012

[22] Katina Michael "Meet Boston dynamics' LS3 - the latest robotic war machine" *The Conversation*, 2012.

[23] Ill-Woo Park, Jung-Yup Kim, Jungho Lee, and Jun-Ho Oh "Online free walking trajectory generation for biped humanoid robot khr-3 (hubo)" *IEEE International Conference on Robotics and Automation*, 2006.

[24] Jung-Yup Kim, Ill-Woo Park, and Jun-Ho Oh "Walking Control Algorithm of Biped Humanoid Robot on Uneven and Inclined Floor" *Journal of Intelligent and Robotic Systems*, 2007.

[25] Jun-ho Oh, David Hanson, Won-sup Kim, Young Han, Jung-yup Kim, and Illwoo Park "Design of Android type Humanoid Robot Albert HUBO" *IEEE/RSJ International Conference on Intelligent Robots and Systems*, 2006.

[26] Marco Hutter and C. David "SLIP running with an articulated robotic leg" *IEEE/RSJ International Conference on Intelligent Robots and Systems*, 2010.

[27] Marc H.Raibert "TROTTING, PACING AND BOUNDING BY A QUADRUPED ROBOT" *Journal of Biomechanics*, 1990.

[28] Austin Shih-Ping Wang, William Wei-Lun Chen, and Pei-Chun Lin "Control of a 2-D bounding passive quadruped model with Poincaré map approximation and model predictive control" *International Conference on Advanced Robotics and Intelligent Systems*, 2016.

[29] Ioannis Poulakakis, Evangelos Papadopoulos, and Martin Buehler "On the Stability of the Passive Dynamics of Quadrupedal Running with a Bounding Gait" *The International Journal of Robotics Research*, 2006.

[30] Ioannis Poulakakis, James Andrew Smith, and Martin Buehler "Modeling and Experiments of Untethered Quadrupedal Running with a Bounding Gait: The Scout II Robot" *The International Journal of Robotics Research*, 2005.

[31] J. Estremera and K. Waldron "Thrust control, stabilization and energetics of a quadruped running robots," *The International Journal of Robotics Research*, 2008.

[32] Y. Fukuoka, H. Kimura, Y. Hada, and K. Takase "Adaptive dynamic walking of a quadruped robot 'Tekken' on irregular terrain using a neural system model" *IEEE International Conference on Robotics and Automation*, 2003.

[33] Hae-Won Park, Sangin Park, and Sangbae Kim "Variable-speed quadrupedal bounding using impulse planning: Untethered high-speed 3D Running of MIT Cheetah 2" *IEEE International Conference on Robotics and Automation*, 2015.

[34] Hae-Won Park, Meng Yee Chuah, and Sangbae Kim "Quadruped bounding control with variable duty cycle via vertical impulse scaling" *IEEE/RSJ International Conference on Intelligent Robots and Systems*, 2014.

[35] Hae-Won Park and Sangbae Kim "Quadrupedal galloping control for a wide range of speed via vertical impulse scaling" *Bioinspiration and biomimetics*, 2015.

[36] Jongwoo Lee, Dong Jin Hyun, Jooeun Ahn, Sangbae Kim, and Neville Hogan "On the dynamics of a quadruped robot model with impedance control: Self-stabilizing high speed trot-running and period-doubling bifurcations" *IEEE/RSJ International Conference on Intelligent Robots and Systems*, 2014.

[37] Max Austin, Jason Brown, Kaylee Geidel, Wenxuan Wang, and Jonathan Clark "Gait design and optimization for efficient running of a direct-drive quadrupedal robot" *Unmanned Systems Technology XIX, 1019504*, 2017.

[38] Jason M. Brown, Charlie P. Carbiener, John Nicholson, Nicholas Hemenway, Jason L. Pusey, and Jonathan Clark "Fore-Aft Leg Specialization Controller for a Dynamic Quadruped" *IEEE International Conference on Robotics and Automation*, 2018.

[39] Gavin Kenneally, Avik De, and D. E. Koditschek "Design Principles for a Family of Direct-Drive Legged Robots" *IEEE Robotics and Automation Letters*, 2016.

[40] Gavin Kenneally and D. E. Koditschek "Leg design for energy management in an electromechanical robot" *IEEE/RSJ International Conference on Intelligent Robots and Systems*, 2015.

[41] Daniel J. Blackman, John V. Nicholson, Camilo Ordonez, Bruce D. Miller, and Jonathan E. Clark "Gait development on Minitaur, a direct drive quadrupedal robot" *Unmanned Systems Technology XVIII, 98370I*, 2016.

[42] Anne E. Martin, David C. Post, and James P. Schmiedeler "The effects of foot geometric properties on the gait of planar bipeds walking under HZD-based control" *The International Journal of Robotics Research*, 2014.

[43] JW Grizzle, G Abba, and F Plestan " Asymptotically stable walking for biped robots: Analysis via systems with impulse effects" *IEEE Transactions on automatic control*, 2001

[44] E.R. Westervelt, J.W. Grizzle, and D.E. Koditschek "Hybrid Zero Dynamics of Planar Biped Walkers" *IEEE Transactions on Automatic Control*, 2003.

[45] Jessy W Grizzle and Christine Chevallereau "Virtual Constraints and Hybrid Zero Dynamics for Realizing Underactuated Bipedal Locomotion" *Cornell University arXiv:1706.01127*, 2017.

[46] Aaron D. Ames, Kevin Galloway, Koushil Sreenath, and Jessy W. Grizzle "Rapidly Exponentially Stabilizing Control Lyapunov Functions and Hybrid Zero Dynamics" *IEEE Transactions on Automatic Control*, 2014.

[47] Qu Cao and Ioannis Poulakakis "Quadrupedal bounding with a segmented flexible torso: passive stability and feedback control" *Bioinspiration and Biomimetics*, 2013.

[48] Qu Cao and Ioannis Poulakakis "Quadrupedal running with a flexible torso: control and speed transitions with sums-of-squares verification" *Artificial Life and Robotics, Springer*, 2016.

[49] Carlos E.García, David M.Prett, and Manfred Morari "Model predictive control: Theory and practice—A survey" *Automatica Volume 25, Issue 3*, 1989.

[50] Gerardo Bledt, Patrick M. Wensing, and Sangbae Kim "Policy-regularized model predictive control to stabilize diverse quadrupedal gaits for the MIT cheetah" *IEEE/RSJ International Conference on Intelligent Robots and Systems*, 2017.

[51] Milton Hildebrand "Motions of the Running Cheetah and Horse" *Journal of Mammalogy, vol. 40, no. 4, pp. 481–495*, 1959.

[52] Martin Golubitsky, Ian Stewart, Pietro-Luciano Buono, and J. J. Collins "Symmetry in locomotor central pattern generators and animal gaits" *Nature volume 401, pages 693–695*, 1999.

[53] Milton Hildebrand "The Quadrupedal Gaits of Vertebrates: The timing of leg movements relates to balance, body shape, agility, speed, and energy expenditure" *BioScience, Volume 39, Issue 11*, 1989.

[54] Felix Ruppert and Alexander Badri-Spröwitz "Series Elastic Behavior of Biarticular Muscle-Tendon Structure in a Robotic Leg" *Frontiers in neurorobotics*, 2019.

[55] Hassan K Khalil. *Nonlinear systems*. Prentice Hall, 2002.

[56] J-J E Slotine and Weiping Li. *Applied nonlinear control*. Prentice Hall, 1991.

[57] Eric Sidorov and Miriam Zacksenhouse "Lyapunov based estimation of the basin of attraction of Poincare maps with applications to limit cycle walking" *Nonlinear Analysis: Hybrid Systems 33 (2019) 179–194*, 2019.

[58] Tingshu Hu and Zongli Lin "On enlarging the basin of attraction for linear systems under saturated linear feedback" *Proceedings of the 2000 American Control Conference*, 2000.

[59] G. Chesi "Computing output feedback controllers to enlarge the domain of attraction in polynomial systems" *IEEE Transactions on Automatic Control*, 2004.

[60] E Vinodh Kumar, Jovitha Jerome, and K. Srikanth "Algebraic approach for selecting the weighting matrices of linear quadratic regulator" *International Conference on Green Computing Communication and Electrical Engineering*, 2014.

[61] Douglas J.Bender and Alan J.Laub "The linear-quadratic optimal regulator for descriptor systems: Discrete-time case" *Automatica Volume 23, Issue 1*, 1987.

[62] Marc H. Raibert "Symmetry in running." *Science 231.4743*, 1986.

[63] Eric R. Westervelt, Jessy W. Grizzle, Christine Chevallereau, Jun Ho Choi, and Benjamin Morris. *Feedback control of dynamic bipedal robot locomotion*. CRC Press, 2007.

[64] Robert D. Gregg and Mark W. Spong. "Reduction-based control of three dimensional bipedal walking robots" *Int. J. Rob. Res., 29(6):680–702*, 2010.

Appendix A

POSITION AND ANGLE OF EACH LINK

Each link's position ((p^h, p^v)) and angle (ϕ) is described by configutation variables. Notation for links are $tor, l^p_{u1}, l^p_{u2}, l^p_{l1}, l^p_{l2}, l^p_f, m^p, b^p, l^a_{u1}, l^a_{u2}, l^a_{l1}, l^a_{l2}, l^a_f, m^a, b^a$. Each link angles, virtual leg length, and virtual leg angle are

$$
\begin{cases}
\phi_{tor} & = q_3 \\
\phi_{l^p_{u1}} & = q_3 - q^p_1 \\
\phi_{l^p_{u2}} & = q_3 - q^p_2 \\
\phi_{l^p_{l1}} & = q_3 - \frac{q^p_1}{2} - \frac{q^p_2}{2} + \frac{3\pi}{2} - cos^{-1}(\frac{l_{l_u}}{l_{l_l}} cos(\frac{q^p_2}{2} - \frac{q^p_1}{2} + \frac{\pi}{2})) \\
\phi_{l^p_f} & = \phi_{l^p_{l1}} \\
\phi^p_{l_{l2}} & = q_3 - \frac{q^p_1}{2} - \frac{q^p_2}{2} - \frac{3\pi}{2} + cos^{-1}(\frac{l_{l_u}}{l_{l_l}} cos(\frac{q^p_2}{2} - \frac{q^p_1}{2} + \frac{\pi}{2})) \\
l^p_v & = (l_{l_l} + l_{l_f})^2 + l^2_{l_u} - l_{l_u} cos(\frac{q^p_2}{2} - \frac{q^p_1}{2} + \frac{\pi}{2} + \sqrt{2l_{l_l} + 2l_{l_f}} cos^{-1}(\frac{l_{l_u}}{l_{l_l}} cos(\frac{q^p_2}{2} - \frac{q^p_1}{2} + \frac{\pi}{2})) \\
\theta^p_v & = q_3 - \frac{q^p_1}{2} - \frac{q^p_2}{2} + \frac{3\pi}{2} - cos^{-1}(\frac{l_{l_u}}{l_{l_l}} sin(\frac{q^p_1}{2} - \frac{q^p_2}{2})) \\
& \quad -cos^{-1}(2(l_{l_l} + l_{l_f})^2 + l_{l_u} sin(\frac{q^p_2}{2} - \frac{q^p_1}{2} + cos^{-1}(\frac{l_{l_u}}{l_{l_l}} sin(\frac{q^p_1}{2} - \frac{q^p_2}{2}))) \times \\
& \quad \sqrt{(l_{l_l} + l_{l_f})^2 + l^2_{l_u} + 2l_{l_u}(l_{l_l} + l_{l_f}) sin(\frac{q^p_2}{2} - \frac{q^p_1}{2} + cos^{-1}(\frac{l_{l_u}}{l_{l_l}} sin(\frac{q^p_1}{2} - \frac{q^p_2}{2}))))}
\end{cases}
\tag{A.1}
$$

$$
\begin{cases}
\phi_{l^a_{u1}} & = q_3 - q^a_1 \\
\phi_{l^a_{u2}} & = q_3 - q^a_2 \\
\phi_{l^a_{l1}} & = q_3 - \frac{q^a_1}{2} - \frac{q^a_2}{2} + \frac{3\pi}{2} - cos^{-1}(\frac{l_{l_u}}{l_{l_l}} cos(\frac{q^a_2}{2} - \frac{q^a_1}{2} + \frac{\pi}{2})) \\
\phi_{l^a_f} & = \phi_{l^a_{l1}} \\
\phi^a_{l_{l2}} & = q_3 - \frac{q^a_1}{2} - \frac{q^a_2}{2} - \frac{3\pi}{2} + cos^{-1}(\frac{l_{l_u}}{l_{l_l}} cos(\frac{q^a_2}{2} - \frac{q^a_1}{2} + \frac{\pi}{2})) \\
l^a_v & = (l_{l_l} + l_{l_f})^2 + l^2_{l_u} - l_{l_u} cos(\frac{q^a_2}{2} - \frac{q^a_1}{2} + \frac{\pi}{2} + \sqrt{2l_{l_l} + 2l_{l_f}} cos^{-1}(\frac{l_{l_u}}{l_{l_l}} cos(\frac{q^a_2}{2} - \frac{q^a_1}{2} + \frac{\pi}{2})) \\
\theta^a_v & = q_3 - \frac{q^a_1}{2} - \frac{q^a_2}{2} + \frac{3\pi}{2} - cos^{-1}(\frac{l_{l_u}}{l_{l_l}} sin(\frac{q^a_1}{2} - \frac{q^a_2}{2})) \\
& \quad -cos^{-1}(2(l_{l_l} + l_{l_f})^2 + l_{l_u} sin(\frac{q^a_2}{2} - \frac{q^a_1}{2} + cos^{-1}(\frac{l_{l_u}}{l_{l_l}} sin(\frac{q^a_1}{2} - \frac{q^a_2}{2}))) \times \\
& \quad \sqrt{(l_{l_l} + l_{l_f})^2 + l^2_{l_u} + 2l_{l_u}(l_{l_l} + l_{l_f}) sin(\frac{q^a_2}{2} - \frac{q^a_1}{2} + cos^{-1}(\frac{l_{l_u}}{l_{l_l}} sin(\frac{q^a_1}{2} - \frac{q^a_2}{2}))))}
\end{cases}
\tag{A.2}
$$

Position of each link is

$$
\begin{cases}
p^p_{l_f} &= [p^h_{l^p_f}, p^v_{l^p_f}]^\top \\
&= [-\frac{l_{l_f}}{2} sin(\frac{q^p_1}{2} - q_3 + \frac{q^p_2}{2} + cos^{-1}(\frac{l_{l_u}}{l_{l_l}} sin(\frac{q^p_1}{2} - \frac{q^p_2}{2}))), \\
&\quad -\frac{l_{l_f}}{2} cos(\frac{q^p_1}{2} - q_3 + \frac{q^p_2}{2} + cos^{-1}(\frac{l_{l_u}}{l_{l_l}} sin(\frac{q^p_1}{2} - \frac{q^p_2}{2})))]^\top \\
p^p_{l_{l1}} &= [p^h_{l_{l1}}, p^v_{l_{l1}}]^\top \\
&= [2p^h_{l^p_f} - \frac{l_{l_l}}{2} sin(\frac{q^p_1}{2} - q_3 + \frac{q^p_2}{2} + cos^{-1}(\frac{l_{l_u}}{l_{l_l}} sin(\frac{q^p_1}{2} - \frac{q^p_2}{2}))), \\
&\quad 2p^v_{l^p_f} - \frac{l_{l_l}}{2} cos(\frac{q^p_1}{2} - q_3 + \frac{q^p_2}{2} + cos^{-1}(\frac{l_{l_u}}{l_{l_l}} sin(\frac{q^p_1}{2} - \frac{q^p_2}{2})))]^\top \\
p^p_{l_{u1}} &= [p^h_{l_{u1}}, p^v_{l_{u1}}]^\top \\
&= [p^h_{l_{l1}} - \frac{l_{l_l}}{2} sin(\frac{q^p_1}{2} - q_3 + \frac{q^p_2}{2} + cos^{-1}(\frac{l_{l_u}}{l_{l_l}} sin(\frac{q^p_1}{2} - \frac{q^p_2}{2}))) - \frac{l_{l_u}}{2} cos(q_3 - q^p_1), \\
&\quad p^v_{l_{l1}} - \frac{l_{l_l}}{2} cos(\frac{q^p_1}{2} - q_3 + \frac{q^p_2}{2} + cos^{-1}(\frac{l_{l_u}}{l_{l_l}} sin(\frac{q^p_1}{2} - \frac{q^p_2}{2}))) - \frac{l_{l_u}}{2} sin(q_3 - q^p_1)]^\top \\
p^p_{l_{l2}} &= [p^h_{l_{l2}}, p^v_{l_{l2}}]^\top \\
&= [2p^h_{l^p_f} - \frac{l_{l_l}}{2} sin(q_3 - \frac{q^p_1}{2} - \frac{q^p_2}{2} + cos^{-1}(\frac{l_{l_u}}{l_{l_l}} sin(\frac{q^p_1}{2} - \frac{q^p_2}{2}))), \\
&\quad 2p^v_{l^p_f} + \frac{l_{l_l}}{2} cos(q_3 - \frac{q^p_1}{2} - \frac{q^p_2}{2} + cos^{-1}(\frac{l_{l_u}}{l_{l_l}} sin(\frac{q^p_1}{2} - \frac{q^p_2}{2})))]^\top \\
p^p_{l_{u2}} &= [p^h_{l_{u2}}, p^v_{l_{u2}}]^\top \\
&= [p^h_{l_{l2}} - \frac{l_{l_l}}{2} sin(q_3 - \frac{q^p_1}{2} - \frac{q^p_2}{2} + cos^{-1}(\frac{l_{l_u}}{l_{l_l}} sin(\frac{q^p_1}{2} - \frac{q^p_2}{2}))) - \frac{l_{l_u}}{2} cos(q_3 - q^p_2), \\
&\quad p^v_{l_{l2}} + \frac{l_{l_l}}{2} cos(q_3 - \frac{q^p_1}{2} - \frac{q^p_2}{2} + cos^{-1}(\frac{l_{l_u}}{l_{l_l}} sin(\frac{q^p_1}{2} - \frac{q^p_2}{2}))) - \frac{l_{l_u}}{2} sin(q_3 - q^p_2)]^\top \\
p_{l_{tor}} &= [p^h_{l_{tor}}, p^v_{l_{tor}}]^\top \\
&= [p^h_{l_{u2}} + \frac{L_{tor}}{2} cos(q_3) - \frac{l_{l_u}}{2} cos(q_3 - q^p_2), p^v_{l_{u2}} + \frac{L_{tor}}{2} sin(q_3) - \frac{l_{l_u}}{2} sin(q_3 - q^p_2)]^\top
\end{cases}
\tag{A.3}
$$

$$
\begin{cases}
p^a_{l_f} & = [p^h_{l^a_f}, p^v_{l^a_f}]^\top \\
& = [-\frac{l_{l_f}}{2} sin(\frac{q^a_1}{2} - q_3 + \frac{q^a_2}{2} + cos^{-1}(\frac{l_{l_u}}{l_{l_l}} sin(\frac{q^a_1}{2} - \frac{q^a_2}{2}))), \\
& \quad -\frac{l_{l_f}}{2} cos(\frac{q^a_1}{2} - q_3 + \frac{q^a_2}{2} + cos^{-1}(\frac{l_{l_u}}{l_{l_l}} sin(\frac{q^a_1}{2} - \frac{q^a_2}{2})))]^\top \\
p^a_{l_{l1}} & = [p^h_{l_{l1}}, p^v_{l_{l1}}]^\top \\
& = [2p^h_{l^a_f} - \frac{l_{l_l}}{2} sin(\frac{q^a_1}{2} - q_3 + \frac{q^a_2}{2} + cos^{-1}(\frac{l_{l_u}}{l_{l_l}} sin(\frac{q^a_1}{2} - \frac{q^a_2}{2}))), \\
& \quad 2p^v_{l^a_f} - \frac{l_{l_l}}{2} cos(\frac{q^a_1}{2} - q_3 + \frac{q^a_2}{2} + cos^{-1}(\frac{l_{l_u}}{l_{l_l}} sin(\frac{q^a_1}{2} - \frac{q^a_2}{2})))]^\top \\
p^a_{l_{u1}} & = [p^h_{l_{u1}}, p^v_{l_{u1}}]^\top \\
& = [p^h_{l_{l1}} - \frac{l_{l_l}}{2} sin(\frac{q^a_1}{2} - q_3 + \frac{q^a_2}{2} + cos^{-1}(\frac{l_{l_u}}{l_{l_l}} sin(\frac{q^a_1}{2} - \frac{q^a_2}{2}))) - \frac{l_{l_u}}{2} cos(q_3 - q^a_1), \\
& \quad p^v_{l_{l1}} - \frac{l_{l_l}}{2} cos(\frac{q^a_1}{2} - q_3 + \frac{q^a_2}{2} + cos^{-1}(\frac{l_{l_u}}{l_{l_l}} sin(\frac{q^a_1}{2} - \frac{q^a_2}{2}))) - \frac{l_{l_u}}{2} sin(q_3 - q^a_1)]^\top \\
p^a_{l_{l2}} & = [p^h_{l_{l2}}, p^v_{l_{l2}}]^\top \\
& = [2p^h_{l^a_f} - \frac{l_{l_l}}{2} sin(q_3 - \frac{q^a_1}{2} - \frac{q^a_2}{2} + cos^{-1}(\frac{l_{l_u}}{l_{l_l}} sin(\frac{q^a_1}{2} - \frac{q^a_2}{2}))), \\
& \quad 2p^v_{l^a_f} + \frac{l_{l_l}}{2} cos(q_3 - \frac{q^a_1}{2} - \frac{q^a_2}{2} + cos^{-1}(\frac{l_{l_u}}{l_{l_l}} sin(\frac{q^a_1}{2} - \frac{q^a_2}{2})))]^\top \\
p^a_{l_{u2}} & = [p^h_{l_{u2}}, p^v_{l_{u2}}]^\top \\
& = [p^h_{l_{l2}} - \frac{l_{l_l}}{2} sin(q_3 - \frac{q^a_1}{2} - \frac{q^a_2}{2} + cos^{-1}(\frac{l_{l_u}}{l_{l_l}} sin(\frac{q^a_1}{2} - \frac{q^a_2}{2}))) - \frac{l_{l_u}}{2} cos(q_3 - q^a_2), \\
& \quad p^v_{l_{l2}} + \frac{l_{l_l}}{2} cos(q_3 - \frac{q^a_1}{2} - \frac{q^a_2}{2} + cos^{-1}(\frac{l_{l_u}}{l_{l_l}} sin(\frac{q^a_1}{2} - \frac{q^a_2}{2}))) - \frac{l_{l_u}}{2} sin(q_3 - q^a_2)]^\top \\
p^a_{l_{tor}} & = [p^h_{l_{tor}}, p^v_{l_{tor}}]^\top \\
& = [p^h_{l_{u2}} + \frac{L_{tor}}{2} cos(q_3) - \frac{l_{l_u}}{2} cos(q_3 - q^a_2), p^v_{l_{u2}} + \frac{L_{tor}}{2} sin(q_3) - \frac{l_{l_u}}{2} sin(q_3 - q^a_2)]^\top
\end{cases}
\tag{A.4}
$$

Jabobian matrix (J) is 4×7 matrix and each component are

$$
\begin{cases}
J(1,1) & = -(l_{l_u} sin(\frac{q_2^p}{2} - \frac{q_1^p}{2} + \frac{\pi}{2} + cos^{-1}((l_{l_u} cos(\frac{q_2^p}{2} - \frac{q_1^p}{2} + \frac{\pi}{2}))/l_{l_l})) \\
& \quad \times((l_{l_u} sin(\frac{q_2^p}{2} - \frac{q_1^p}{2} + \frac{\pi}{2}))/(2l_{l_l}(-(l_{l_u}^2 cos(-\frac{q_1^p}{2} + \frac{q_2^p}{2} + \frac{\pi}{2})^2)/l_{l_l}^2 + 1)^{\frac{1}{2}}) + \frac{1}{2}) \\
& \quad \times(2l_{l_l} + 2l_{l_f}))/(2((l_{l_l} + l_{l_f})^2 + l_{l_u}^2 - l_{l_u} cos(-\frac{q_1^p}{2} + \frac{q_2^p}{2} + \frac{\pi}{2} \\
& \quad + cos^{-1}((l_{l_u} cos(-\frac{q_1^p}{2} + \frac{q_2^p}{2} + \frac{\pi}{2}))/l_{l_l}))(2l_{l_l} + 2l_{l_f}))^{\frac{1}{2}}) \\
J(1,2) & = (l_{l_u} sin(\frac{q_2^p}{2} - \frac{q_1^p}{2} + \frac{\pi}{2} + cos^{-1}((l_{l_u} cos(\frac{q_2^p}{2} - \frac{q_1^p}{2} + \frac{\pi}{2}))/l_{l_l})) \\
& \quad ((l_{l_u} sin(\frac{q_2^p}{2} - \frac{q_1^p}{2} + \frac{\pi}{2}))/(2l_{l_l}(-(l_{l_u}^2 cos(-\frac{q_1^p}{2} + \frac{q_2^p}{2} + \frac{\pi}{2})^2)/l_{l_l}^2 + 1)^{\frac{1}{2}}) + \frac{1}{2}) \\
& \quad \times(2l_{l_l} + 2l_{l_f}))/(2((l_{l_l} + l_{l_f})^2 + l_{l_u}^2 \\
& \quad - l_{l_u} cos(-\frac{q_1^p}{2} + \frac{q_2^p}{2} + \frac{\pi}{2} + cos^{-1}((l_{l_u} cos(-\frac{q_1^p}{2} + \frac{q_2^p}{2} + \frac{\pi}{2}))/l_{l_l}))(2l_{l_l} + 2l_{l_f}))^{\frac{1}{2}}) \\
J(1,3:7) & = 0 \\
J(2,1) & = (l_{l_u} sin(\frac{q_2^p}{2} - \frac{q_1^p}{2} + \frac{\pi}{2}))/(2l_{l_l}(-(l_{l_u}^2 cos(-\frac{q_1^p}{2} + \frac{q_2^p}{2} + \frac{\pi}{2})^2)/l_{l_l}^2 + 1)^{\frac{1}{2}}) \\
& \quad -((l_{l_u} sin(\frac{q_2^p}{2} - \frac{q_1^p}{2} + \frac{\pi}{2} + cos^{-1}((l_{l_u} cos(\frac{q_2^p}{2} - \frac{q_1^p}{2} + \frac{\pi}{2}))/l_{l_l})) \\
& \quad \times((l_{l_u} sin(\frac{q_2^p}{2} - \frac{q_1^p}{2} + \frac{\pi}{2}))/(2l_{l_l}(-(l_{l_u}^2 cos(-\frac{q_1^p}{2} + \frac{q_2^p}{2} + \frac{\pi}{2})^2)/l_{l_l}^2 + 1)^{\frac{1}{2}}) + \frac{1}{2})) \\
& \quad /((l_{l_l} + l_{l_f})^2 + l_{l_u}^2 - l_{l_u} cos(-\frac{q_1^p}{2} + \frac{q_2^p}{2} + \frac{\pi}{2} \\
& \quad + cos^{-1}((l_{l_u} cos(-\frac{q_1^p}{2} + \frac{q_2^p}{2} + \frac{\pi}{2}))/l_{l_l}))(2l_{l_l} + 2l_{l_f}))^{\frac{1}{2}} - (l_{l_u} sin(\frac{q_2^p}{2} - \frac{q_1^p}{2} + \frac{\pi}{2} \\
& \quad + cos^{-1}((l_{l_u} cos(\frac{q_2^p}{2} - \frac{q_1^p}{2} + \frac{\pi}{2}))/l_{l_l}))(2(l_{l_l} + l_{l_f})^2 - l_{l_u} cos(\frac{q_2^p}{2} - \frac{q_1^p}{2} + \frac{\pi}{2} \\
& \quad + cos^{-1}((l_{l_u} cos(\frac{q_2^p}{2} - \frac{q_1^p}{2} + \frac{\pi}{2}))/l_{l_l}))(2l_{l_l} + 2l_{l_f}))((l_{l_u} sin(\frac{q_2^p}{2} - \frac{q_1^p}{2} + \frac{\pi}{2})) \\
& \quad /(2l_{l_l}(-(l_{l_u}^2 cos(-\frac{q_1^p}{2} + \frac{q_2^p}{2} + \frac{\pi}{2})^2)/l_{l_l}^2 + 1)^{\frac{1}{2}}) + \frac{1}{2})) \\
& \quad /(2((l_{l_l} + l_{l_f})^2 + l_{l_u}^2 - l_{l_u} cos(-\frac{q_1^p}{2} + \frac{q_2^p}{2} + \frac{\pi}{2} + cos^{-1}((l_{l_u} cos(-\frac{q_1^p}{2} + \frac{q_2^p}{2} + \frac{\pi}{2})) \\
& \quad /l_{l_l}))(2l_{l_l} + 2l_{l_f}))^{\frac{3}{2}}))/(-(2(l_{l_l} + l_{l_f})^2 - l_{l_u} cos(-\frac{q_1^p}{2} + \frac{q_2^p}{2} + \frac{\pi}{2} \\
& \quad + cos^{-1}((l_{l_u} cos(-\frac{q_1^p}{2} + \frac{q_2^p}{2} + \frac{\pi}{2}))/l_{l_l}))(2l_{l_l} + 2l_{l_f}))^2/((2l_{l_l} + 2l_{l_f})^2((l_{l_l} + l_{l_f})^2 \\
& \quad + l_{l_u}^2 - l_{l_u} cos(-\frac{q_1^p}{2} + \frac{q_2^p}{2} + \frac{\pi}{2} + cos^{-1}((l_{l_u} cos(-\frac{q_1^p}{2} + \frac{q_2^p}{2} + \frac{\pi}{2}))/l_{l_l})) \\
& \quad \times(2l_{l_l} + 2l_{l_f}))) + 1)^{\frac{1}{2}} - \frac{1}{2}
\end{cases}
\tag{A.5}
$$

$$
\begin{cases}
J(2,2) & = ((l_{l_u} sin(\frac{q_2^p}{2} - \frac{q_1^p}{2} + \frac{\pi}{2} + cos^{-1}((l_{l_u} cos(\frac{q_2^p}{2} - \frac{q_1^p}{2} + \frac{\pi}{2}))/l_{l_l})) \\
& \quad \times((l_{l_u} sin(\frac{q_2^p}{2} - \frac{q_1^p}{2} + \frac{\pi}{2}))/(2l_{l_l}(-(l_{l_u}^2 cos(-\frac{q_1^p}{2} + \frac{q_2^p}{2} + \frac{\pi}{2})^2)/l_{l_l}^2 + 1)^{\frac{1}{2}}) + \frac{1}{2})) \\
& \quad /((l_{l_l} + l_{l_f})^2 + l_{l_u}^2 - l_{l_u} cos(-\frac{q_1^p}{2} + \frac{q_2^p}{2} + \frac{\pi}{2} \\
& \quad + cos^{-1}((l_{l_u} cos(-\frac{q_1^p}{2} + \frac{q_2^p}{2} + \frac{\pi}{2}))/l_{l_l}))(2l_{l_l} + 2l_{l_f}))^{\frac{1}{2}} \\
& \quad -(l_{l_u} sin(\frac{q_2^p}{2} - \frac{q_1^p}{2} + \frac{\pi}{2} + cos^{-1}((l_{l_u} cos(\frac{q_2^p}{2} - \frac{q_1^p}{2} + \frac{\pi}{2}))/l_{l_l})) \\
& \quad \times(2(l_{l_l} + l_{l_f})^2 - l_{l_u} cos(\frac{q_2^p}{2} - \frac{q_1^p}{2} + \frac{\pi}{2} + cos^{-1}((l_{l_u} cos(\frac{q_2^p}{2} - \frac{q_1^p}{2} + \frac{\pi}{2})/l_{l_l})) \\
& \quad \times(2l_{l_l} + 2l_{l_f}))((l_{l_u} sin(\frac{q_2^p}{2} - \frac{q_1^p}{2} + \frac{\pi}{2})) \\
& \quad /(2l_{l_l}(-(l_{l_u}^2 cos(-\frac{q_1^p}{2} + \frac{q_2^p}{2} + \frac{\pi}{2})^2)/l_{l_l}^2 + 1)^{\frac{1}{2}}) + \frac{1}{2})) \\
& \quad /(2((l_{l_l} + l_{l_f})^2 + l_{l_u}^2 - l_{l_u} cos(-\frac{q_1^p}{2} + \frac{q_2^p}{2} + \frac{\pi}{2} \\
& \quad + cos^{-1}((l_{l_u} cos(-\frac{q_1^p}{2} + \frac{q_2^p}{2} + \frac{\pi}{2}))/l_{l_l})) \\
& \quad \times(2l_{l_l} + 2l_{l_f}))^{\frac{3}{2}}))/(-(2(l_{l_l} + l_{l_f})^2 - l_{l_u} cos(-\frac{q_1^p}{2} + \frac{q_2^p}{2} + \frac{\pi}{2} \\
& \quad + cos^{-1}((l_{l_u} cos(-\frac{q_1^p}{2} + \frac{q_2^p}{2} + \frac{\pi}{2}))/l_{l_l})) \\
& \quad \times(2l_{l_l} + 2l_{l_f}))^2/((2l_{l_l} + 2l_{l_f})^2((l_{l_l} + l_{l_f})^2 + l_{l_u}^2 - l_{l_u} cos(-\frac{q_1^p}{2} + \frac{q_2^p}{2} + \frac{\pi}{2} \\
& \quad + cos^{-1}((l_{l_u} cos(-\frac{q_1^p}{2} + \frac{q_2^p}{2} + \frac{\pi}{2}))/l_{l_l})) \\
& \quad \times(2l_{l_l} + 2l_{l_f}))) + 1)^{\frac{1}{2}} - (l_{l_u} sin(\frac{q_2^p}{2} - \frac{q_1^p}{2} + \frac{\pi}{2})) \\
& \quad /(2l_{l_l}(-(l_{l_u}^2 cos(-\frac{q_1^p}{2} + \frac{q_2^p}{2} + \frac{\pi}{2})^2)/l_{l_l}^2 + 1)^{\frac{1}{2}}) - \frac{1}{2} \\
J(2,3) & = 0 \\
J(2,4) & = 1 \\
J(2,5:7) & = 0 \\
J(3,1:2) & = 0 \\
J(3,3) & = -(l_{l_u} sin(\frac{q_2^a}{2} - \frac{q_1^a}{2} + \frac{\pi}{2} + cos^{-1}((l_{l_u} cos(\frac{q_2^a}{2} - \frac{q_1^a}{2} + \frac{\pi}{2}))/l_{l_l})) \\
& \quad \times((l_{l_u} sin(\frac{q_2^a}{2} - \frac{q_1^a}{2} + \frac{\pi}{2}))/(2l_{l_l}(-(l_{l_u}^2 cos(-\frac{q_1^a}{2} + \frac{q_2^a}{2} + \frac{\pi}{2})^2)/l_{l_l}^2 + 1)^{\frac{1}{2}}) + \frac{1}{2}) \\
& \quad \times(2l_{l_l} + 2l_{l_f}))/(2((l_{l_l} + l_{l_f})^2 + l_{l_u}^2 - l_{l_u} cos(-\frac{q_1^a}{2} + \frac{q_2^a}{2} + \frac{\pi}{2} \\
& \quad + cos^{-1}((l_{l_u} cos(-\frac{q_1^a}{2} + \frac{q_2^a}{2} + \frac{\pi}{2}))/l_{l_l}))(2l_{l_l} + 2l_{l_f}))^{\frac{1}{2}})
\end{cases}
\tag{A.6}
$$

$$
\begin{cases}
J(3,4) & = (l_{l_u} sin(\frac{q_2^a}{2} - \frac{q_1^a}{2} + \frac{\pi}{2} + cos^{-1}((l_{l_u} cos(\frac{q_2^a}{2} - \frac{q_1^a}{2} + \frac{\pi}{2}))/l_{l_l})) \\
& \quad \times((l_{l_u} sin(\frac{q_2^a}{2} - \frac{q_1^a}{2} + \frac{\pi}{2}))/(2l_{l_l}(-(l_{l_u}^2 cos(-\frac{q_1^a}{2} + \frac{q_2^a}{2} + \frac{\pi}{2})^2) \\
& \quad /l_{l_l}^2 + 1)^{\frac{1}{2}}) + \frac{1}{2})(2l_{l_l} + 2l_{l_f})) \\
& \quad /(2((l_{l_l} + l_{l_f})^2 + l_{l_u}^2 - l_{l_u} cos(-\frac{q_1^a}{2} + \frac{q_2^a}{2} + \frac{\pi}{2} \\
& \quad + cos^{-1}((l_{l_u} cos(-\frac{q_1^a}{2} + \frac{q_2^a}{2} + \frac{\pi}{2}))/l_{l_l}))(2l_{l_l} + 2l_{l_f}))^{\frac{1}{2}}) \\
J(3,5:7) & = 0 \\
J(4,1:2) & = 0 \\
J(4,3) & = (l_{l_u} sin(\frac{q_2^a}{2} - \frac{q_1^a}{2} + \frac{\pi}{2}))/(2l_{l_l}(-(l_{l_u}^2 cos(-\frac{q_1^a}{2} + \frac{q_2^a}{2} + \frac{\pi}{2})^2)/l_{l_l}^2 + 1)^{\frac{1}{2}}) \\
& \quad -((l_{l_u} sin(\frac{q_2^a}{2} - \frac{q_1^a}{2} + \frac{\pi}{2} + cos^{-1}((l_{l_u} cos(\frac{q_2^a}{2} - \frac{q_1^a}{2} + \frac{\pi}{2}))/l_{l_l})) \\
& \quad \times((l_{l_u} sin(\frac{q_2^a}{2} - \frac{q_1^a}{2} + \frac{\pi}{2}))/(2l_{l_l}(-(l_{l_u}^2 cos(-\frac{q_1^a}{2} + \frac{q_2^a}{2} + \frac{\pi}{2})^2)/l_{l_l}^2 + 1)^{\frac{1}{2}}) + \frac{1}{2})) \\
& \quad /((l_{l_l} + l_{l_f})^2 + l_{l_u}^2 - l_{l_u} cos(-\frac{q_1^a}{2} + \frac{q_2^a}{2} + \frac{\pi}{2} + cos^{-1}((l_{l_u} cos(-\frac{q_1^a}{2} + \frac{q_2^a}{2} + \frac{\pi}{2})) \\
& \quad /l_{l_l}))(2l_{l_l} + 2l_{l_f}))^{\frac{1}{2}} - (l_{l_u} sin(\frac{q_2^a}{2} - \frac{q_1^a}{2} + \frac{\pi}{2} + cos^{-1}((l_{l_u} cos(\frac{q_2^a}{2} - \frac{q_1^a}{2} + \frac{\pi}{2}))/l_{l_l})) \\
& \quad \times(2(l_{l_l} + l_{l_f})^2 - l_{l_u} cos(\frac{q_2^a}{2} - \frac{q_1^a}{2} + \frac{\pi}{2} + cos^{-1}((l_{l_u} cos(\frac{q_2^a}{2} - \frac{q_1^a}{2} + \frac{\pi}{2}))/l_{l_l})) \\
& \quad \times(2l_{l_l} + 2l_{l_f}))((l_{l_u} sin(\frac{q_2^a}{2} - \frac{q_1^a}{2} + \frac{\pi}{2})) \\
& \quad /(2l_{l_l}(-(l_{l_u}^2 cos(-\frac{q_1^a}{2} + \frac{q_2^a}{2} + \frac{\pi}{2})^2)/l_{l_l}^2 + 1)^{\frac{1}{2}}) + \frac{1}{2}))/(2((l_{l_l} + l_{l_f})^2 + l_{l_u}^2 \\
& \quad - l_{l_u} cos(-\frac{q_1^a}{2} + \frac{q_2^a}{2} + \frac{\pi}{2} + cos^{-1}((l_{l_u} cos(-\frac{q_1^a}{2} + \frac{q_2^a}{2} + \frac{\pi}{2}))/l_{l_l})) \\
& \quad \times(2l_{l_l} + 2l_{l_f}))^{\frac{3}{2}}))/(-(2(l_{l_l} + l_{l_f})^2 - l_{l_u} cos(-\frac{q_1^a}{2} + \frac{q_2^a}{2} + \frac{\pi}{2} \\
& \quad + cos^{-1}((l_{l_u} cos(-\frac{q_1^a}{2} + \frac{q_2^a}{2} + \frac{\pi}{2}))/l_{l_l}))(2l_{l_l} + 2l_{l_f}))^2/((2l_{l_l} + 2l_{l_f})^2((l_{l_l} + l_{l_f})^2 \\
& \quad + l_{l_u}^2 - l_{l_u} cos(-\frac{q_1^a}{2} + \frac{q_2^a}{2} + \frac{\pi}{2} + cos^{-1}((l_{l_u} cos(-\frac{q_1^a}{2} + \frac{q_2^a}{2} + \frac{\pi}{2}))/l_{l_l})) \\
& \quad \times(2l_{l_l} + 2l_{l_f}))) + 1)^{\frac{1}{2}} - \frac{1}{2}
\end{cases}
\tag{A.7}
$$

$$
\begin{cases}
J(4,4) & = ((l_{l_u} sin(\frac{q_2^a}{2} - \frac{q_1^a}{2} + \frac{\pi}{2} + cos^{-1}((l_{l_u} cos(\frac{q_2^a}{2} - \frac{q_1^a}{2} + \frac{\pi}{2}))/l_{l_l})) \\
& \quad \times((l_{l_u} sin(\frac{q_2^a}{2} - \frac{q_1^a}{2} + \frac{\pi}{2}))/(2l_{l_l}(-(l_{l_u}^2 cos(-\frac{q_1^a}{2} + \frac{q_2^a}{2} + \frac{\pi}{2})^2)/l_{l_l}^2 + 1)^{\frac{1}{2}}) + \frac{1}{2})) \\
& \quad /((l_{l_l} + l_{l_f})^2 + l_{l_u}^2 - l_{l_u} cos(-\frac{q_1^a}{2} + \frac{q_2^a}{2} + \frac{\pi}{2} \\
& \quad + cos^{-1}((l_{l_u} cos(-\frac{q_1^a}{2} + \frac{q_2^a}{2} + \frac{\pi}{2}))/l_{l_l})) \\
& \quad \times(2l_{l_l} + 2l_{l_f}))^{\frac{1}{2}} - (l_{l_u} sin(\frac{q_2^a}{2} - \frac{q_1^a}{2} + \frac{\pi}{2} + cos^{-1}((l_{l_u} cos(\frac{q_2^a}{2} - \frac{q_1^a}{2} + \frac{\pi}{2}))/l_{l_l})) \\
& \quad \times(2(l_{l_l} + l_{l_f})^2 - l_{l_u} cos(\frac{q_2^a}{2} - \frac{q_1^a}{2} + \frac{\pi}{2} + cos^{-1}((l_{l_u} cos(\frac{q_2^a}{2} - \frac{q_1^a}{2} + \frac{\pi}{2}))/l_{l_l})) \\
& \quad \times(2l_{l_l} + 2l_{l_f}))((l_{l_u} sin(\frac{q_2^a}{2} - \frac{q_1^a}{2} + \frac{\pi}{2})) \\
& \quad /(2l_{l_l}(-(l_{l_u}^2 cos(-\frac{q_1^a}{2} + \frac{q_2^a}{2} + \frac{\pi}{2})^2)/l_{l_l}^2 + 1)^{\frac{1}{2}}) + \frac{1}{2}))/(2((l_{l_l} + l_{l_f})^2 \\
& \quad + l_{l_u}^2 - l_{l_u} cos(-\frac{q_1^a}{2} + \frac{q_2^a}{2} + \frac{\pi}{2} + cos^{-1}((l_{l_u} cos(-\frac{q_1^a}{2} + \frac{q_2^a}{2} + \frac{\pi}{2}))/l_{l_l})) \\
& \quad \times(2l_{l_l} + 2l_{l_f}))^{\frac{3}{2}}))/(-(2(l_{l_l} + l_{l_f})^2 - l_{l_u} cos(-\frac{q_1^a}{2} + \frac{q_2^a}{2} + \frac{\pi}{2} \\
& \quad + cos^{-1}((l_{l_u} cos(-\frac{q_1^a}{2} + \frac{q_2^a}{2} + \frac{\pi}{2}))/l_{l_l})) \\
& \quad \times(2l_{l_l} + 2l_{l_f}))^2/((2l_{l_l} + 2l_{l_f})^2((l_{l_l} + l_{l_f})^2 + l_{l_u}^2 \\
& \quad - l_{l_u} cos(-\frac{q_1^a}{2} + \frac{q_2^a}{2} + \frac{\pi}{2} + cos^{-1}((l_{l_u} cos(-\frac{q_1^a}{2} + \frac{q_2^a}{2} + \frac{\pi}{2}))/l_{l_l})) \\
& \quad \times(2l_{l_l} + 2l_{l_f}))) + 1)^{\frac{1}{2}} - (l_{l_u} sin(\frac{q_2^a}{2} - \frac{q_1^a}{2} + \frac{\pi}{2})) \\
& \quad /(2l_{l_l}(-(l_{l_u}^2 cos(-\frac{q_1^a}{2} + \frac{q_2^a}{2} + \frac{\pi}{2})^2)/l_{l_l}^2 + 1)^{\frac{1}{2}}) - \frac{1}{2} \\
J(4,5) & = 1 \\
J(4,6:7) & = 0
\end{cases}
\tag{A.8}
$$

Appendix B

ESTIMATED BASIN OF ATTRACTION

Estimated basin of attraction is described by variables which are differences of current state and initial state at fixed point ($x_c^{p*} = [q_1^{p*}, q_2^{p*}, q_3^*, \dot{q}_1^{*p}, \dot{q}_2^{*p}, \dot{q}_3^*]^\top$).

$$\begin{aligned} x &= x_c^p - x_c^{p*} = [x_1, x_2, x_3, x_4, x_5, x_6]^\top \\ &= [q_1^p - q_1^{p*}, q_2^p - q_2^{p*}, q_3 - q_3^*, \dot{q}_1^p - \dot{q}_1^{*p}, \dot{q}_2^p - \dot{q}_2^{*p}, \dot{q}_3 - \dot{q}_3^*]^\top \end{aligned} \tag{B.1}$$

Estimated basin of attraction has form

$$V(x) \leq \rho \tag{B.2}$$

B.1 VPP Controlled Bounding Gait with Adjusted Input Set

B.1.1 v_x = 0.8 m/s

$V_{0.8} = 1.7346x_1^2 + 0.9881x_1x_2 + 0.0964x_1x_3 + 0.0242x_1x_4 - 0.0033x_1x_5 - 0.0034x_1x_6 + 2.1354x_2^2 - 2.4055x_2x_3 - 0.0201x_2x_4 + 0.1507x_2x_5 + 0.1644x_2x_6 + 0.7986x_3^2 + 0.0283x_3x_4 - 0.0855x_3x_5 - 0.1308x_3x_6 + 0.0009x_4^2 + 0.0001x_4x_5 - 0.0053x_4x_6 + 0.0034x_5^2 + 0.0030x_5x_6 + 0.0089x_6^2$

$\rho_{0.8} = 0.4967$

B.1.2 v_x = 1.15 m/s

$V_{1.15} = 4.1045x_1^2 + 0.3979x_1x_2 + 1.1558x_1x_3 + 0.1064x_1x_4 - 0.0757x_1x_5 - 0.2321x_1x_6 + 34.2965x_2^2 - 31.4145x_2x_3 - 0.5016x_2x_4 + 1.5290x_2x_5 + 2.6369x_2x_6 + 7.9219x_3^2 + 0.2649x_3x_4 - 0.7448x_3x_5 - 1.2932x_3x_6 + 0.0060x_4^2 - 0.0067x_4x_5 - 0.0411x_4x_6 + 0.0219x_5^2 + 0.0477x_5x_6 + 0.0797x_6^2$

$\rho_{1.15} = 10.0017$

B.1.3 v_x = 1.2 m/s

$V_{1.2} = 11.1406x_1^2 + 0.7988x_1x_2 + 1.1119x_1x_3 + 0.2398x_1x_4 - 0.1344x_1x_5 - 0.5801x_1x_6 + 11.3877x_2^2 - 9.2611x_2x_3 - 0.0795x_2x_4 + 0.1334x_2x_5 + 0.3979x_2x_6 + 2.0621x_3^2 + 0.0485x_3x_4 - 0.0734x_3x_5 - 0.2034x_3x_6 + 0.0025x_4^2 - 0.0135x_4x_6 + 0.0024x_5^2 + 0.0012x_5x_6 + 0.0188x_6^2$

$\rho_{1.2} = 1.1672$

B.1.4 v_x = 1.4 m/s

$V_{1.4} = 9.8643x_1^2 - 2.5453x_1x_2 - 1.6771x_1x_3 + 0.4351x_1x_4 + 0.0530x_1x_5 - 1.2303x_1x_6 + 9.4908x_2^2 + 1.7415x_2x_3 + 0.4101x_2x_4 + 0.0453x_2x_5 - 1.1331x_2x_6 + 3.4662x_3^2 + 0.0758x_3x_4 - 0.1672x_3x_5 - 0.2725x_3x_6 + 0.0362x_4^2 + 0.0666x_4x_5 - 0.1760x_4x_6 + 0.0665x_5^2 - 0.1235x_5x_6 + 0.2242x_6^2$

$\rho_{1.4} = 9.0646$

B.1.5 v_x = 1.6 m/s

$V_{1.6} = 45.3577x_1^2 - 3.3951x_1x_2 - 4.8180x_1x_3 + 1.6975x_1x_4 - 0.2389x_1x_5 - 4.9018x_1x_6 + 39.9887x_2^2 - 12.7119x_2x_3 + 0.1054x_2x_4 - 2.6116x_2x_5 - 1.4078x_2x_6 + 8.4207x_3^2 - 0.1828x_3x_4 - 0.0941x_3x_5 + 0.5707x_3x_6 + 0.0555x_4^2 + 0.0870x_4x_5 - 0.2876x_4x_6 + 0.1361x_5^2 - 0.1392x_5x_6 + 0.3911x_6^2$

$\rho_{1.6} = 9.3400$

B.1.6 v_x = 1.75 m/s

$V_{1.75} = 6.5988x_1^2 + 0.8922x_1x_2 - 3.5576x_1x_3 + 0.3827x_1x_4 - 0.0148x_1x_5 - 1.1418x_1x_6 + 7.6774x_2^2 + 3.6869x_2x_3 + 0.2386x_2x_4 - 0.2398x_2x_5 - 0.7082x_2x_6 + 6.3716x_3^2 - 0.1452x_3x_4 - 0.2902x_3x_5 + 0.4476x_3x_6 + 0.0253x_4^2 + 0.0471x_4x_5 - 0.1322x_4x_6 + 0.0515x_5^2 - 0.1013x_5x_6 + 0.1777x_6^2$

$\rho_{1.75} = 9.7076$

B.1.7 v_x = 2.05 m/s

$V_{2.05} = 14.1960x_1^2 - 0.5034x_1x_2 - 8.6085x_1x_3 + 0.8133x_1x_4 + 0.0881x_1x_5 - 2.3529x_1x_6 + 37.4264x_2^2 - 6.3309x_2x_3 + 0.3208x_2x_4 - 1.3220x_2x_5 - 0.7782x_2x_6 + 7.1070x_3^2 - 0.5347x_3x_4 -$

$0.3333x_3x_5+1.5933x_3x_6+0.0267x_4^2+0.0329x_4x_5-0.1520x_4x_6+0.0534x_5^2-0.0823x_5x_6+0.2188x_6^2$

$\rho_{2.05} = 25.0002$

B.1.8 v_x = 2.25 m/s

$V_{2.25} = 2.8539x_1^2+0.8429x_1x_2-1.3206x_1x_3+0.1346x_1x_4-0.0346x_1x_5-0.3754x_1x_6+2.1275x_2^2-1.1468x_2x_3+0.0873x_2x_4+0.0506x_2x_5-0.2142x_2x_6+2.0377x_3^2-0.0991x_3x_4-0.0692x_3x_5+0.3227x_3x_6+0.0059x_4^2+0.0066x_4x_5-0.0347x_4x_6+0.0082x_5^2-0.0169x_5x_6+0.0516x_6^2$

$\rho_{2.25} = 2.6977$